NTNU

Norwegian University of
Science and Technology

Design of a Permanently Magnetized Hypocycloidal Reluctance Machine

Adapting the rolling rotor concept to generator and converter operation

Åsmund Kleiva Nilsen

Master of Science in Energy and Environment
Submission date: June 2011
Supervisor: Robert Nilssen, ELKRAFT

Norwegian University of Science and Technology
Department of Electric Power Engineering

Design of a New Permanent Magnetized Hypocycloidal Reluctance Machine

Åsmund K. Nilsen, Student, NTNU and Robert K. Nilssen, Professor, NTNU

***Abstract*—A new prototype of a Hypocycloid Reluctance Machine is designed, the purpose of the prototype is generator operation for low rpm - high torque application. The design incorporates NdFeB-magnets to provide the magnetization, and it's torque potential benefits from converter operation. Theoretical potential of the machine is explored, and two different simulation models, based FEM and magnetic circuit, are built to calculate the torque potential specifically for the prototype. The process of building the prototype machine is started.**

***Index Terms*—PMHRM, hypocycloidal machine, reluctance machine, high torque, PM machine**

I. Introduction

THIS article proposes a new design of the hypocycloidal, or rolling rotor, machine suited to novel application as generator, and with full converter drive - the PMHRM. Lengthy derivation and calculations are in general placed in the appendices together with description of the simulation models, to keep the main part of the article as concise as possible.

The hypocycloidal, or rolling rotor, electrical machine was first described by Russian engineer A.I. Moskowitin in 1944, and further investigated by Austrian R. Schön [1]. The machine utilizes the magnetic field in radial direction in contrary to standard machines which utilizes the tangential field component. In theory, the stronger radial flux gives the motor an excellent torque per volume, making it suitable as a replacement for geared high-speed motors. Absence of a fast rotating mass and a gear reduces the motors inertia, resulting very fast dynamic characteristics for the machine.

In the 1960s a design called the Steromotor was patented and tried commercialized by M.C. Rosain and G. Stcherbatcheff. This machine has been the basis for thorough analysis on the rolling rotor concept.[2]. Some studies have focused on improving the Steromotor-design by using more complex current control, with [3] and without [4] converters.

With earlier studies of the machine focused on a wound stator solution, this project aims to use permanent magnets to magnetize the machine. Permanently magnetizing the stator can be ideal for generator use of the machine, but some changes must be made. After investigations into the nature of the HRM, and how to permanently magnetize it, a design is proposed. Based on this design, work is started to construct a specific prototype. Models of this specific prototype are built for FEM and magnetic circuit analysis.

Contents

II. Theory

This section aims to give a theoretical insight to the PMHR-machine's functionality. For more detailed derivations on the general rolling rotor concept, readers are referred to *"Aspects of the hypocycloidal reluctance motor"* by R.A. Ashen and H.R. Bolton [2]. Additional considerations have been made in the preliminary study.[5]

A. Working principle

The essence of the hypocycloidal machine is the cylindrical stator, and a non-salient, eccentrically placed rotor. The principle of reluctance minimization is the driving force in the machine. Whenever there is magnetic field in the air gap, forces will act on the rotor. If the magnetic field is unbalanced, the forces too will be unbalanced and cause movement. To create clockwise movement, referred to fig. 1, the magnetic field in the blue section must be stronger than the field in the red section. If the field is controlled to advance in front of the

List of symbols

E_f	:	excitation voltage/back emf
e	:	eccentricity
G	:	gear ratio
g	:	air gap length
k_r	:	radius of rotor (bearings)
l	:	machine length/depth
r_r	:	outer radius of rotor (magnetic part)
r_s	:	inner radius of stator
R	:	rotor ratio, r_r/r_s
T	:	torque
X_{ar}	:	armature reactance
α	:	degrees around the rotor
γ	:	locus of the total reluctance forces on the rotor
μ_0	:	primary magnetic constant
Φ_m	:	flux from magnet linking to coil
Φ_r	:	remanent flux in the PMs
ψ	:	current leading angle
$\Re_g$	:	reluctance of air gap
$\Re_s$	:	reluctance of stator (leakage gap and magnet gap in parallell)
σ	:	Maxwell's stress tensor
Θ	:	angular position of contact point (minimum air gap) between rotor and stator, referred to stator center
ω_r	:	angular velocity of motor output shaft
ω_s	:	angular velocity of stator magnetic field, and velocity of rotor gyration.

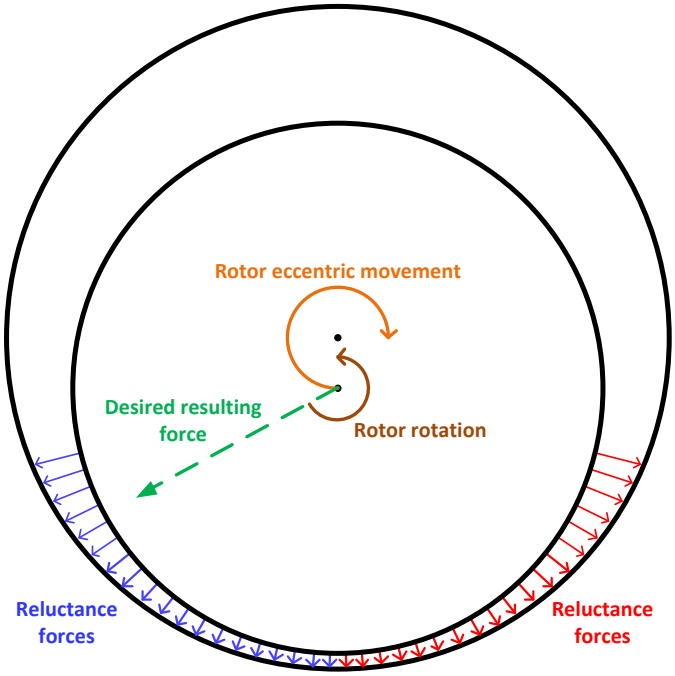

Fig. 1: Cross section view of magnetic part of the PMHR

rotor-stator contact point, the rotor will continuously travel the inner perimeter of the stator.

Forces acting on the rotor can be assumed normal on it's surface. When forces along the rotor surface are integrated, the resulting force on the rotor can be decomposed into a force working through a line from the rotor centre and the stator-rotor contact point, and a force acting normal on this line. The latter component causes the movement, while the normal component causes friction. This friction between the rotor and stator spins the rotor with a direction opposite of the stator field rotation.

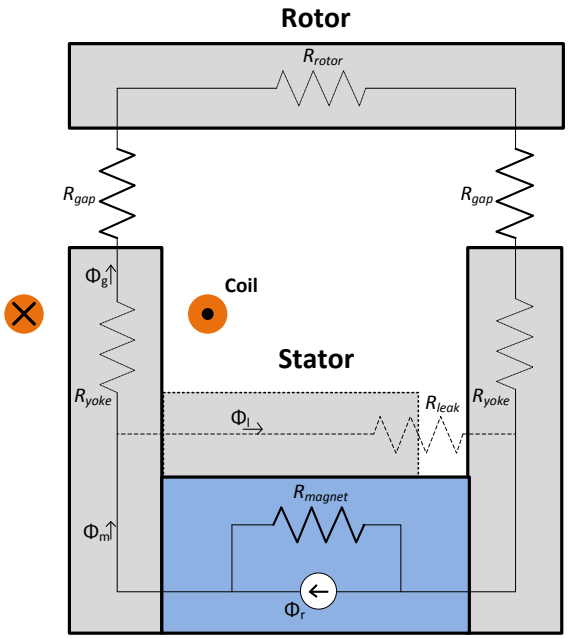

Fig. 2: One actuator unit / stator section

In this project, friction between rotor and stator is created in mechanical bearings fitted to the machine, this way there is no need for contact between the electromagnetic parts and wear is reduced.

B. PM magnetizing and the necessary leakage path

Magnetizing of the hypocycloid machines has traditionally been done with coils. This project relies on permanent magnetization. The permanent magnets will set up a balanced field around the rotor, and coils will be necessary to manipulate the field or react to shaft movement. With the insertion of PM, the reluctance of the coil's flux path increases, and it's ability to manipulate the field torque is drastically reduced. This problem is solved using actuator principles. A large leakage leg/path is introduced, reducing the need for ampere-turns to manipulate the field. This also allows a full neutralization of the field in the air gap without reducing the field in the PM to a dangerously low level.

While permanent magnets seems ideal to magnetize the machine for generator operation, it is not necessarily useful for motor operation. When the machine is running as a motor, there is no need for magnetization or armature reaction. The only aim is to produce a magnetic field in the air gap. Since the permanent magnets only set up a balanced field, the current needed to produce field in lead of the contact point is reduced, it is increased correspondingly in order to neutralize the field in the wake of the motor. It boils down to how the coils are controlled. For motor operation with individual control of the coils, the permanent magnets add nothing but cost and reluctance to the stator. When the reluctance problem is overcome with the leakage gap, it results in an increased stator volume. If bidirectional currents (typically sinusoidal) are run in the coil, the permanent magnets will provide the DC bias to

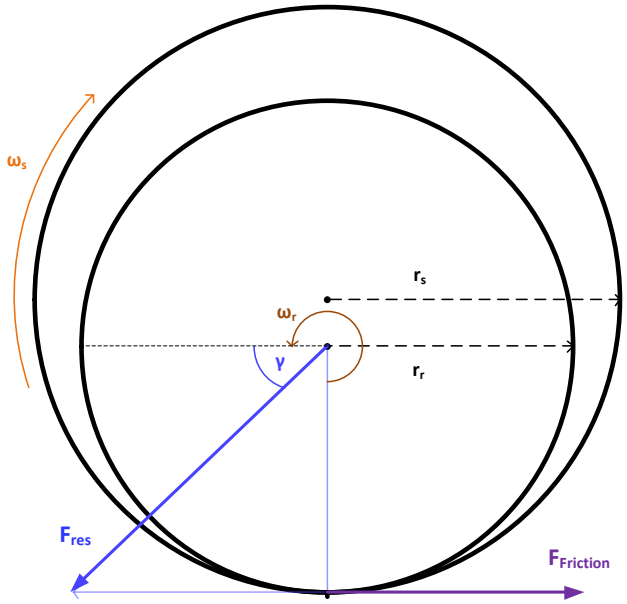

Fig. 3: Simplified sketch of mechanical parts of machine

needed neutralize the field in the wake of the motor, increasing the torque.

The stator consists of several actuator units, with two oppositely magnetized teeth, placed in series around it's circumference. See [5] for detailed sketches more of the stator. Figure 2 shows a single stator unit. The flux from the permanent magnets has two alternative routes; through the rotor and through a leakage leg. As the rotor moves, R_{gap} changes and the magnetizing flux commutates from the air gap to the leakage gap and back again, inducing a voltage in the coil.

C. Gearing and eccentricity

The mechanical energy is extracted or inserted in the machine at the slow rotating rotor shaft. An expression for the angular speed of the rotor, given by angular speed of the field in stator and the rotor and stator radius can be found. Figure 3 shows the machine represented at the mechanical bearings and there is no minimum air gap as required between the magnetic active parts.

For each cycle, the rotor with a radius r_r covers a distance equal to the inner perimeter of the stator, r_s. The distance is covered by the two components of movement, the epicyclic vibratory motion and the rotor rotation. If there is no slip, eq.1 is valid and an expression for the gearing ratio can be deducted.

$$\omega_s * 2\pi r_s = \omega_s * 2\pi k_r + w_r * 2\pi k_r \tag{1}$$

$$G = \frac{\omega_r}{\omega_s} = \frac{r_s - k_r}{k_r} \tag{2}$$

Eccentricity is defined a little differently in study than in other literature, as the distance between rotor and stator centre.

$$\epsilon = r_s - (r_r + g_{min}) \tag{3}$$

D. Theoretic torque potential

The torque potential of the conventional Steromotor has been determined[2]. Three phase operation allows the machine to operate at saturation and maximum air gap density only at one point in the machine. With individual control of the actuators, however, it is possible to increase the field to a maximum value in all parts of the air gap desired.

Torque can be expressed as the total force normal to the line between rotor centre and the contact point, multiplied with the rotor radius.

$$T = F * cos\gamma * k_r \tag{4}$$

An estimate for maximum obtainable torque within some restrictions can be made. Field density is 1.6 Tesla in the whole region 135° in front of the contact point,Θ. The field is limited in strength by saturation in the iron, and in extension by the friction requirement. A component of the force must act from the rotor centre through the contact point. Magnetic forces is the integral of the Maxwell's stress tensor. For the HRM-design the stress tensor can be simplified to:

$$\sigma = \frac{1}{2\mu_0} B(\alpha)^2 \tag{5}$$

If α is mechanical degrees around the rotor, total force and torque can then be expressed as

$$Fcos\gamma = \frac{1}{2\mu_0} r_r l \int_0^{\frac{3}{4}\pi} B(\alpha)^2 sin\alpha d\alpha \tag{6}$$

$$T = \frac{1}{2\mu_0} k_r r_r l \int_0^{\frac{3}{4}\pi} 1.6^2 sin\alpha d\alpha \tag{7}$$

The torque density per rotor swept volume can then be found by dividing eq. 7 on volume. Eq. 8 is simplified by setting r_r = k_r, and $r_r = r_s$, possible in an ideal design.

$$\bar{T} = \frac{1}{\pi k_r^2 l} \frac{1}{2\mu_0} k_r r_r l \mu_0 \int_0^{\frac{3}{4}\pi} 1.6^2 sin\alpha d\alpha \tag{8}$$

$$\bar{T} = \frac{1}{2\pi\mu_0} \int_0^{\frac{3}{4}\pi} 1.6^2 sin\alpha d\alpha = 5.535 * 10^5 Nm/m^3 \tag{9}$$

This figure will be hard to achieve in a practical solution. Stator volume may have to be increased to avoid saturation. Keeping a high field where the gap length increases requires a lot of current and copper losses will mount if maximal torque potential is to be extracted.

The theoretical potential of the Steromotor under traditional three-phase operation have been determined to $2.86 * 10^5 Nm/m^3$ [2]. This figure is achieved at a maximal flux density of only 1.2T, but does not ensure the necessary forces to create friction. The Steromotor also has a passive mid-region that is not included in the calculation. Given the same conditions, the individually controlled machine has a potential of $3.65 * 10^5 Nm/m^3$. Clearly, achieving a high flux density in the air gap is crucial.

E. Torque versus power density

In this section the need for a minimum air gap is disregarded. $k_r = r_r$. Rotor ratio, R, is defined as r_r/r_s.

Seen from eq. 7 increasing the rotor by a factor k causes the torque to increase by a factor k^2. It is common for HR-machines to define the torque density with respect to rotor swept volume. Rotor swept volume is defined by the stator inner radius. Torque density will increase with a factor k^2 as R increases towards unity.

As the rotor radius increases, the air gaps in the machine decreases. This means less magnetomotive force is required to magnetize the machine, reducing the need for PM and copper volume. The stator volume can thus be decreased, and the torque density referred to total motor volume increases with a factor of more than k^2 as rotor diameter is increased within the stator radius. If torque density is the only concern, rotor ratio should be as close to unity as practically possible.

While torque density increases with larger rotor ratio, power dwindles as rotation speed decreases. For applications, a certain amount of power is needed. Using eqs.2 and 4, an expression can be set up.

$$\begin{aligned} P &= T\omega_r \qquad (10)\\ &= T\omega_s \frac{r_s - r_r}{r_r}\\ &\propto r_r r_s - r_r^2\\ \bar{P} &\propto \frac{r_r r_s - r_r^2}{r_s^2} = R - R^2 \qquad (11) \end{aligned}$$

Maximal power density is then found at R = 0.5, illustrating that, even though torque potential is the reason for choosing a HRM, some torque has to be sacrificed to meet the power (and speed) requirement.

F. Electric operation

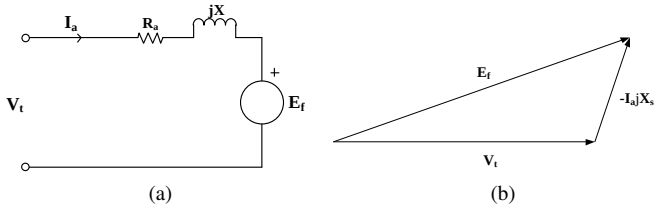

Fig. 4: a) Per phase equivalent of machine b) Phasors, generator operation

A per coil equivalent for the machine can be set up as in fig. 4a. Both the excitation voltage and the reactance is distinguished because of the rotors eccentricity.

The excitation voltage can be defined as

$$E_f = N\frac{d\Phi_m}{dt} = k * \omega_s \frac{d\left(\Phi_r * \frac{\Re_s}{\Re_s + \Re_g}\right)}{dt} \qquad (12)$$

The air gap reluctance is commonly approximated proportional to $sin(\Theta)$[2], this is close enough for relevant values of R. According to eq.12, the excitation voltage will then vary with the inverse of $k + sin(\Theta)$. Clearly this does not give a sinusoidal voltage. (Simulation results are shown in sec. IV.)

The armature reactance, which is dominant, can be expressed by eq.13, and is not sinusoidal either.

$$X_{ar} = \omega \frac{N^2}{\Re s + \Re_g} \qquad (13)$$

Leakage reactance, outside of the intended leakage leg, will also vary and be considerable when the rotor air gap is large.

With a non-sinusoidal excitation voltage, and varying inductance, the phasor diagram in fig.4b is artificial. However, it does illustrate the difficulty of providing a reasonable terminal voltage. Sinusoidal or square wave operation will give current and torque pulsations.

Because of the rotors eccentricity, using a regular dq-axis approach becomes difficult. If one is to define a q-axis for the machine, it will be the angle in front of the contact point at where to place the current space vector to in order to produce the highest $Fcos\gamma$. This angle, ψ, is found numerically in the magnetic model analysis. It is dependent on rotor ratio and magnetic loading in the stator.

III. Design and construction of a prototype

This chapter focuses on the practical aspects of incorporating the PM and flux switching features into the HR-machine. Fitting of the electromagnetic and mechanical parts, and providing the eccentric shaft arrangement is looked into here. More details are found in appendix A. The machine is still under manufacture when this report is submitted.

A. Mechanical parts

It was decided to use cog wheels as mechanical bearings to avoid slip and ensure predictable operation. To keep costs down, the shelf availability of cog wheel set limits to the physical variables. Two different inner cog wheels were ordered, one to be sure of successful operation, the other to give better performance.

The outer cog wheel has a contact diameter of 200mm and 100 teeth, the two inner cog wheels have a contact diameter of 180mm and 90 teeth, and 190mm and 95 teeth respectively. From eq. 2, this corresponds to a gearing ratio of 9 and 19.

Cog wheels interacting creates a separation force in the point of contact. These forces will be overcome by the magnetic attraction forces in the electromagnetic part of the machine. But the cost is that energy is drained from the magnetic field, resulting in lower torque density and efficiency. To avoid this it is desirable with a bearing arrangement to absorb the separation forces created between the gears. A sliding bearing can be used at the back of the machine at the end of the shaft. In the front of the machine, at the power outtake/inlet, a double roller bearing arrangement, where the inner roller bearing is axially displaced within the outer bearing can be used.

To provide the torque transmission and filtering of the rotor shaft's eccentric movement, two angular joints were ordered. The joints are intended to operate on a small angle to reduce losses and wear.

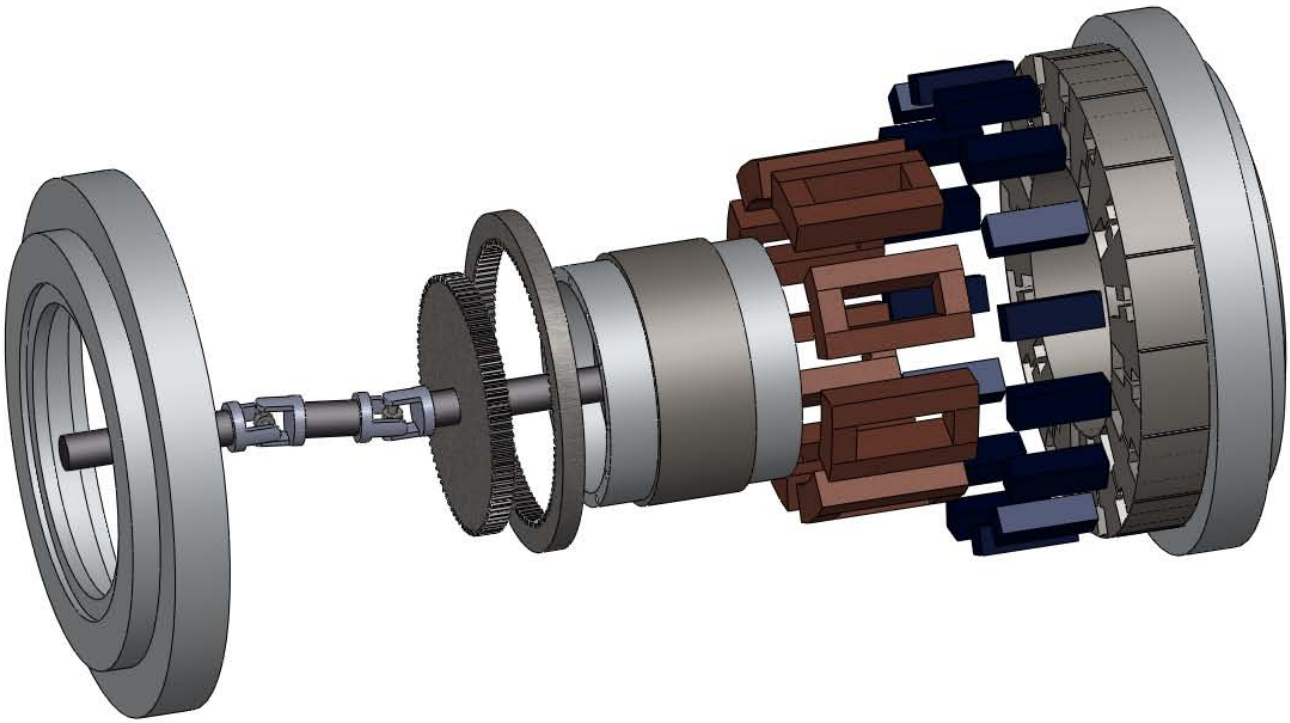

Fig. 5: Exploded view of important motor parts

B. Electromagnetic parts

The stator laminations were designed with CAD-software and produced by LCD Lasercut. Magnets were delivered by Neorem Magnets. The rotor and the coils are produced at NTNU.

While the sizes of the rotor and stator were free to choose, the eccentricity (distance from rotor centre to stator centre) was limited by the mechanical bearings to 10mm and 5mm for the two cog wheels respectively. To achieve maximal flux linkage a small minimum air gap is desirable. However, with uncertainties in the tooling process and the rigidity of the assembly, a safety margin and minimum air gap of 0.5 mm was set to ensure proper operation. The stator was set to have a inner diameter of 200mm. To accomplish the safety margin the electromagnetical rotor has to have a 1mm shorter diameter than the rotor cog wheel contact diameter.

Fig. 6 shows a stator lamination cross section. The stator consists of eight separate actuator units. Permanent magnets will be mounted with north pole facing in towards the central leg. With PM magnetization only, every other stator tooth is a north or south pole seen from the rotor. The stator was designed with flux concentration to utilize that forces are proportional to the magnetic field squared, this also leaves rectangular slots for the windings.

From the producer the stator was ordered with 1mm wide struts between each pole section to ease the assembly in the workshop. These struts were to be removed after assembly. Tolerances from the manufacturer are relatively small for the lamination cutting, only 0.02 mm. The magnets might require larger tolerance, and it was decided to go for a total tolerance of 0.1mm in total in the magnet slots. This is not considered to be much.

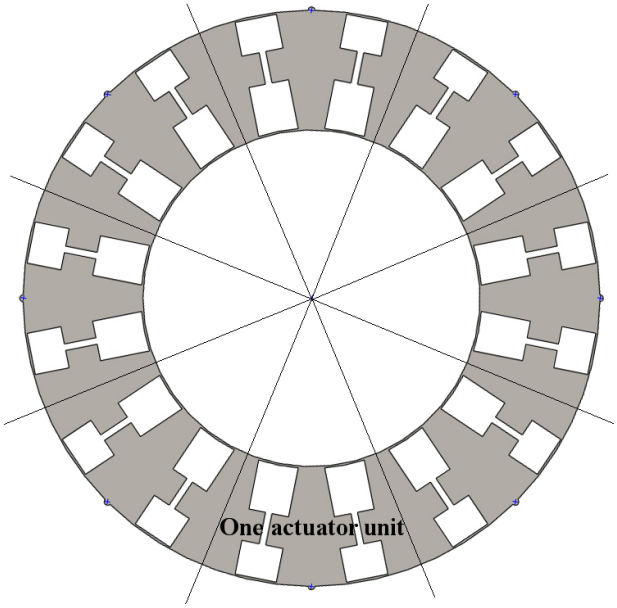

Fig. 6: Stator lamination

The machine had to be of a suitable size to work with. With a depth of 7cm and the stator lamination diameter at 342mm, it ended up a little heavy. The length of the leakage gap had to be substantially longer than the minimum air gap, stealing as little as the PM-flux as possible at minimum air

gap, but at the same time short enough to allow a the coil to react properly without an insane number of turns. After the stator lamination parameters were decided, the coils and the magnets were designed to match each other in the given stator. The magnet is perhaps surprisingly long, with a length of 25mm in the direction of magnetization. It is required for the magnet to operate at a decent point with the rather large eccentricity and leakage gap.

C. Assembly

To assemble the machine, supports, spacers and a rig are needed. Care must be taken not to divert any of the PM-field from it's intended path. The leakage leg gaps in the stator were filled with non-magnetic, supportive material. To give room for the coils, spacers are needed between the electromagnetic stator and the outer cog wheel. These spacers wraps around the stator, restricting it from expanding radially. Spacers of similar length are placed between EM-rotor and cog wheel to align the rotor with the stator. A main frame is needed to support the machine and the shaft arrangement. Drawings are found in appendix A.

It is the intention that the rotor can be replaced in a later stage, altering eccentricity and machine characteristics. The assembly design must allow replacement of the parts necessary to change rotor and mechanical bearings. This means that bolting, or other reversible fastening, is preferred to glue in critical interfaces.

IV. Analysis on magnetic model

A magnetic model of the PMHRM was built with the aim to determine inductances, voltage shapes and the torque potential of the machine. A sketch of the magnetic equivalent of the machine is shown in figure 7, a nodal matrix was set up for this equivalent and used as a basis for the calculations. A script was built in MatLab to do the calculations. For details the magnetic analysis, see appendix B.

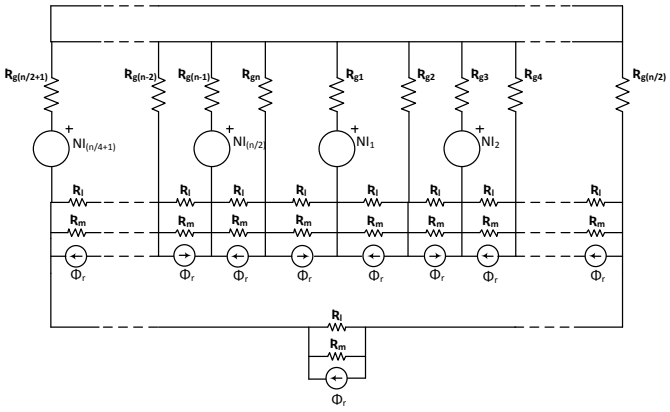

Fig. 7: Generic equivalent of the HSRPM-machine

A. Inductances and PM-linkage

The analysis showed that coil self inductance and the flux linkage from the PM to the coils are dominating. Mutual contributions from other coils play a very small part of the total inductance. Fig. 8 shows the inductances and PM-flux linkage for a machine with rotor diameter of 189mm.

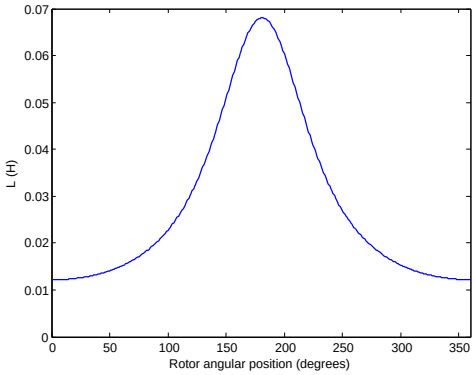

(a)

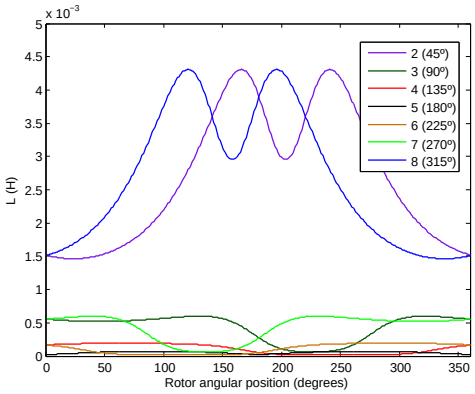

(b)

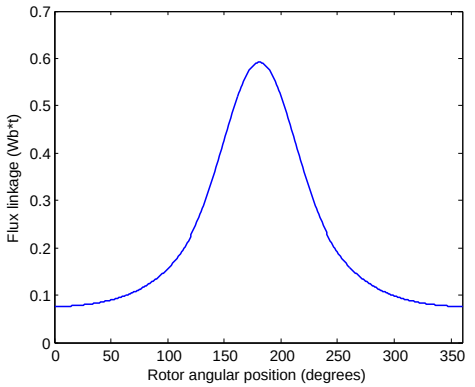

(c)

Fig. 8: a) Self inductance b) Mutual inductances c) PM flux linkage

B. Induced voltages

With no hysteresis loss, the induced voltage is proportional the rotational speed, or frequency, of the machine. Table I shows the voltages obtained with a output shaft rotation of speed 63rpm, corresponding to 20Hz. The voltages are drawn in fig. 9

As shown in fig. 9a, the induced voltage from a single coil is close to zero for a large portion of the period. A lot of

TABLE I: Voltages induced at $\omega_{mech} = 63rpm$

	V_{peak}	V_{RMS}	*f(Hz)*
Single coil	59.4	20.6	20
Two coil phase	81.4	33.3	”
Four coil phase	90.2	40.6	”
Opposite coils	56.9	31.5	40

the voltage, and thereby power density, is lost when coupling coils in series. With the non sinusoidal the voltage will contain harmonics. One possible improvement to this is to couple opposite coils together as in fig. 9d, resulting in a doubling of the frequency.

C. Torque Potential

Torque calculations were done from the co-energy approach, setting the current to standard currents schemes. This means amounts of reactive power will be needed to achieve the following torque, higher copper losses and converter rating will increase. The handling of the co-energy is not foolproof, and results would benefit from verification. Results are presented in table II. The highest torque potential is given by a current control where the coils are at positive rated current in front of the rotor, and switched to negative rated current right after the rotor. The torque density for the 189mm version is $1.01 * 10^5 Nm/m^3$. (Torque to rotor swept volume). Torque ripple during a period is a problem which is best handled by a 8-phase operation. It is likely that the ripple found is enhanced by the lumped parameter approach of the magnetic model. The air gaps are in reality distributed and will smooth some transitions. The abrupt switching in the I_{rated} on/off scheme will nonetheless cause great ripple.

Creating a machine with a slot number not a multiple of three made it difficult to do a sensible analysis of three phase layout as no symmetrical three phase winding can be laid out.

Torque to rotor position, Θ, for the 189mm version is shown in fig. 10. The value on the Y-axis must be multiplied with gearing ratio to give the torque at the rotor shaft.

Simulations verified that torque potential was drastically reduced without a leakage path in the stator.

TABLE II: Torque potential of the prototype under different control schemes and rotors

Current operation	**Torque (Nm)**		**Ripple pk-pk (Nm)**	
Rotor:	*189mm*	*179mm*	*189mm*	*179mm*
I_{rated} on/off	223	111	60.3	88.8
3-phase	136	59	200.5	111.2
8-phase	174	77	7.9	12.4

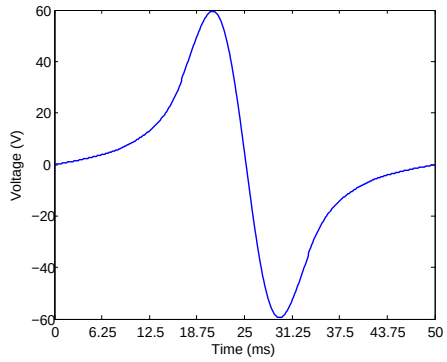

(a)

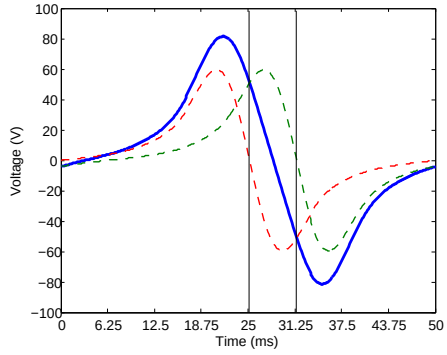

(b)

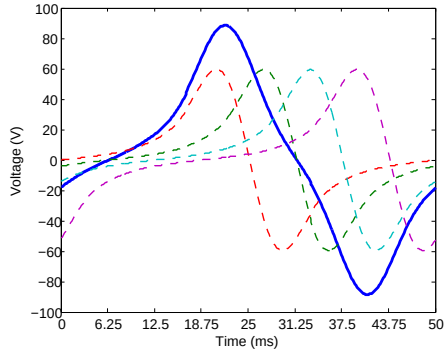

(c)

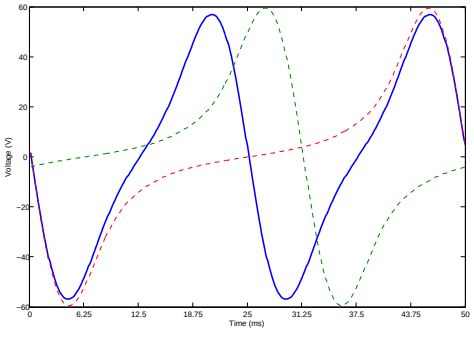

(d)

Fig. 9: a) Single coil b) Two neighbouring coils c) Four neighbour coils d) Two opposite coils

D. Problems and issues with the magnetic model

There was found a bias in the calculation, with a cogging torque averaging at 1.3 Nm over a full period. This indicates that there will be some error margin in other results too. The magnetic model is lumped. For a machine with 16 teeth, air gap length will vary along each tooth, this is not considered in the lumped parameter model. The switching of coils from

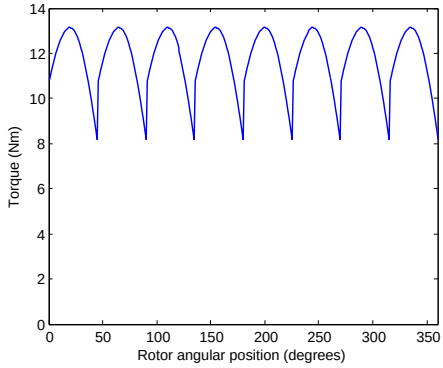

(a)

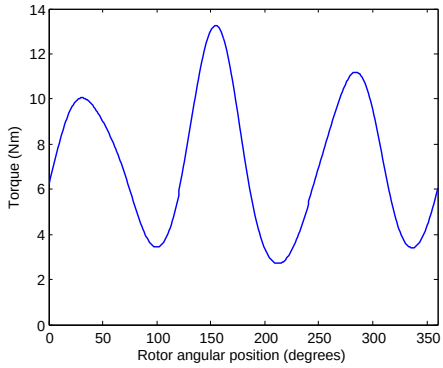

(b)

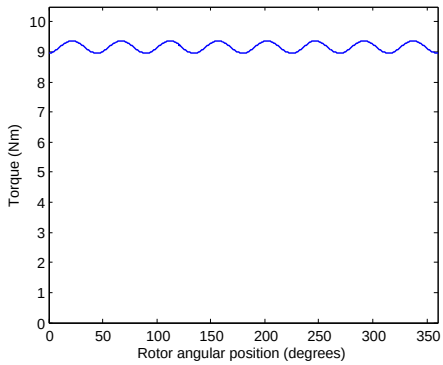

(c)

Fig. 10: Torque with a) I_{rated} on/off b) Three phase c) Eight phase

positive to negative current will also cause an extra brutal ripple. An exact, correct expression for co-energy was not found, and a scaling factor had to be used when. This might prove to give errors. An alternative would be to use the script to find the air gap flux and approximate the torque.

V. FEM-ANALYSIS

A FEM-model of the PMHR-machine has been built. A stationary FEM-analysis has been conducted on model to investigate levels of saturation and to attempt a verification of the torque in the machine. Efforts were also made to do a time dependent study of the rotating machine, with the aim to verify and compare the results found through the magnetic model in sec. IV. These efforts were not successful, however, and no

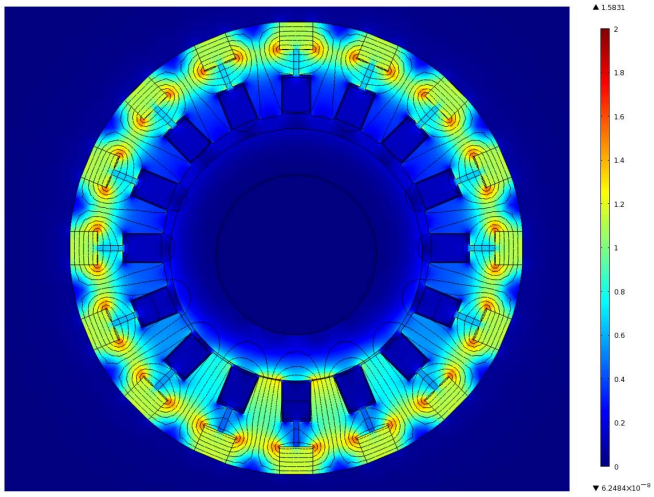

(a)

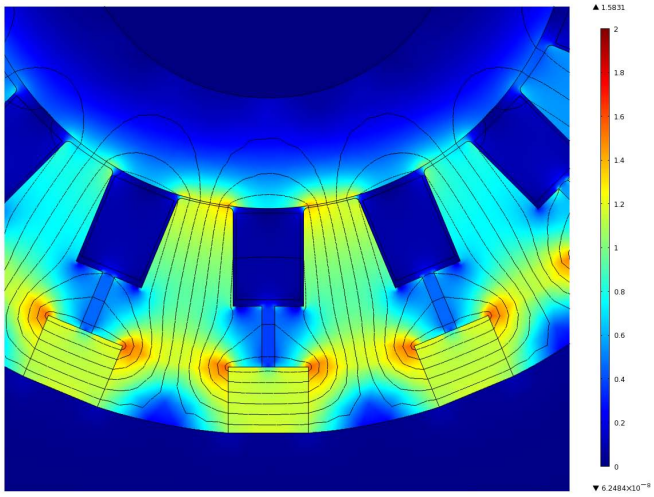

(b)

Fig. 11: Only PM load a) Full view b) Detailed view

valuable results produced. The stationary analysis shows that the iron is saturated in the teeth when maximum current is run, and a small part of the magnet could be demagnetized in temperatures above 150, degrees. Torque estimations are around 150Nm for the 189mm rotor, and 70Nm for the 179mm rotor, with considerably more ripple for the 179mm rotor. For more and details about on the FEM-model, see appendix C.

A. Stationary study

A model of the machine was built in the Rotating Machinery-module of COMSOL. For both rotors, the field distribution was investigated. In fig. 11 only the PM contribute to the field. For a heavier saturation, FEM-analysis was also done with several coils delivering maximum current, simulating a maximum torque motor operation. The field distribution in this critical case is shown in fig. 12. Both plots show the rotor at $\Theta = 348.75$.

The highest level of saturation is in the central tooth at minimum air gap, with close to 2.4 Tesla. With a sinusoidal

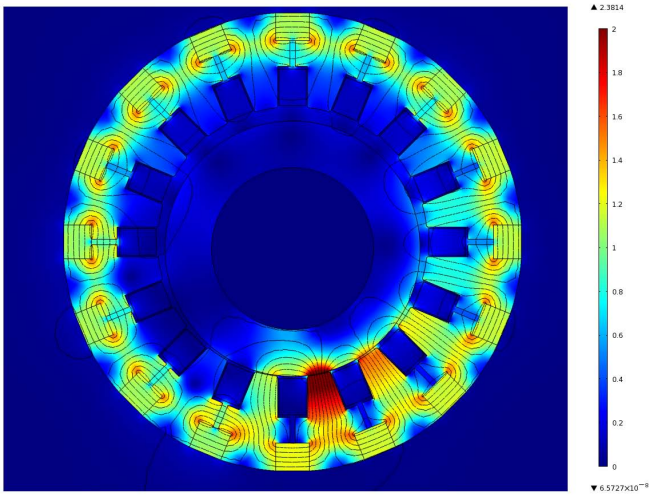

(a)

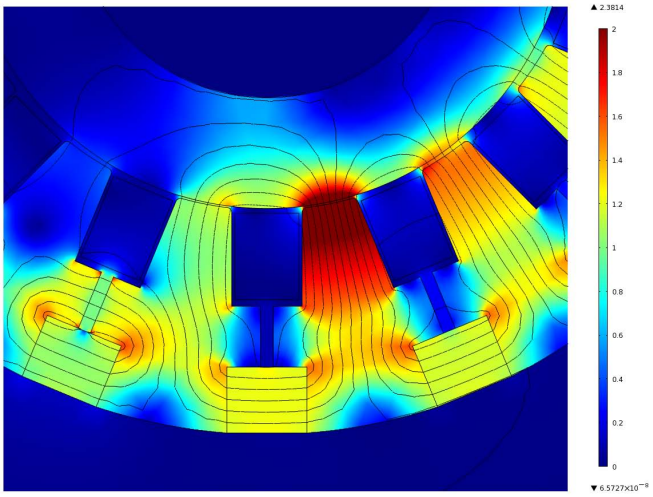

(b)

Fig. 12: Current load: a) Full view b) Detailed view

current leading on the minimum air gap, the stress will be considerably reduced, as maximum current occurs before mininum air gap and the flux contributions from the coil and the PMs will not peak at the same time. For the magnet the most critical point is when the coil works to pacify the unit at small air gaps. The flux from the leakage leg travels into the magnet reducing the field down to the non-linear area for temperatures above 150 degrees. For PM-magnetization curve see fig. 18.

One way to approximate torque on the rotor is to integrate the component of the force on the rotor tangential to the contact point, and then multiplying with the arm of from the contact point to the rotor centre. By doing several stationary analysis, and moving the rotor slightly between each of the analysis, an impression the torque as a function of position can be given. One must remember that no field history or hysteresis is taken into account here, but it is the best alternative as long the time dependent study is not solved.

The results of the torque analysis is found in tab. III. Rotor

TABLE III: Torque at different rotor positions

	Torque (Nm)	
Rotor offset (deg)	*189mm*	*179mm*
-11.25	154.02	75.11
0	137.46	58.02
11.25	151.59	73.26
22.5	150.93	84.66
33.75	153.77	75.02

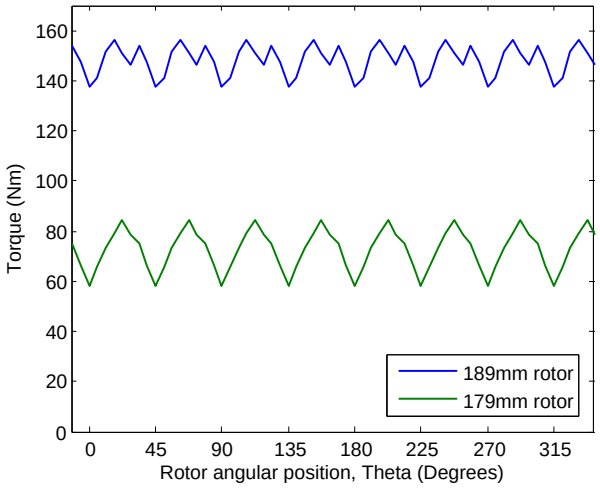

Fig. 13: Torque during a period, 189mm rotor

offset equals Θ, the central leg of the first unit/coil is at $\Theta = 0$.

The results in tab. III covers a Θ sector of 45 degrees, by recognizing the symmetry and that this pattern will repeat for every of the eight units, a graph for the torque produced in the machine is presented in fig. 13. (The figure builds on more points than presented in tab. III.)

B. Time dependent study

Problems were encountered with the rotating model. Small air-gap, eccentricity and the material unlinearity required a fine mesh and heavy computation muscles. Different simplifications were applied, but with limited computational power no acceptable solution was not found within the time at disposal. COMSOL-support, represented by Bertil Nistad, identified the problem to be a too coarse mesh in the current build.

One possible solution can be to set up the mesh across the air gap as radial bands of triangular elements. Using this method, a finnish-polish team succeeded at solving studies on a HRM-with very small air gaps.[6]

The current build set up for rotational movement can be found through the ENO-group at the Department of Electric Power Engineering.

VI. Results and Discussion

In this section results of the analysis looked into and compared to theory. Experiences from the building process are also discussed.

A. Torque

Finite element and magnet circuit analysis give different results. Torque density of the prototype is 6-18% of potential optimistically derived in sec. II-D. Changing rotor radius affects the torque potential in a predictable manner.

A summary of the results from the torque studies is found in table IV.

TABLE IV: Torque and torque density found in studies

Study	**Torque (Nm)**		**T. density** (kN/m^2)	
	189mm	*179mm*	*189mm*	*179mm*
FEM	150	72	67	35
Magnetic circuit	223	111	101	50

When comparing the torque found in the COMSOL-model and through the magnetic circuit model, there is a clear difference. The magnetic circuit model gives a torque 50% higher for the 189mm rotor, and 54% higher for the 179mm rotor. Until verification by testing, the COMSOL-simulation should be trusted the most as a professional tool. Several explanations for the deviations can be found. Field leakage, except from the intended leakage leg, is not included for in the magnetic circuit model. The magnetic model can be more detailed. Also, there are large uncertainties around the torque-calculation in the MC-model and the scaling factor there. It seems like the second scaling factor discussed in sec. B-E is the better alternative. The ripple is also larger in the MC-model This can partly be explained by the lumped approach, where every air gap is considered as a point. In reality, the distribution of the airgaps will smooth out transitions in the air gap minimum region.

Comparing the results for the 189mm rotor to the theoretical maximum found in sec. II-D, show that the machine achieves only 12% (FEM) and 18% (MC) of the theoretical torque potential. The results for the 179Nm-version is 6.5% (FEM) and 9.0% (MC)

Looking at the field distribution in the machine in sec. V it is clear that a flux density of 1.6 Tesla is not obtained all sectors of the air gap. The magnetic loading is reduced to give room for copper. Since air gaps become large, the PM and the coils are not able create a large field at $\alpha > 45\,\mathrm{deg}$. To achieve a higher flux density in all sectors one may either increase PM and copper volume in stator, or increase the rotor ratio, as discussed in sec. II-E.

If looking at the torque produced by the prototype of J. Reinert *et al.*[3], it was found to have a torque density of $62kNm/m^3$, very close to FEM results for the 189mm-version in this project. Running at lower speed, it is assumed that the former machine has a higher gearing ratio.

Between the two rotors, the difference in torque density is in accordance with the theory. Rotor ratio is increased by a factor 1.055, and most important the stator is able to create a larger magnetic field in the smaller airgap of the 189mm machine. The torque increase also corresponds well when compared to input power (current) and gearing ratio. Torque ripple is remarkably higher with the 179mm version, this is due to the low number of actuator units. With the larger air gaps in the 179mm-version, fewer actuators give a substantial torque contribution at the same time. Compared to the individual contributions from each coil in fig. 34a, the torque peaks of each coil in the 179mm machine are smaller narrower.

B. Voltage

Scaling up the results for induced voltage found in tab. I to a rotational speed of 157.5rpm on the shaft and 50Hz in the stator, each coil will have an excitation voltage of 148.5V peak and 51.5V RMS. These numbers are for the 189mm version of the machine, and especially the RMS value will be reduced for the 179mm-version. The voltage is to low for practical purposes, and higher current must be used.

C. Practical aspects

The use of cog wheels as mechanical bearings has proved to put restrictions on obtainable torque. Three phase operation of a machine with concentrated coils and a number of slots not divisible on three is problematic. Filtering the eccentric movement from the rotor shaft can be done in a multiple of ways.

It was decided to use cog wheels as mechanical bearings, as it will give predictable operation with no slip. Problems arose with the set of cog wheels first intended for use, as they interlocked. With smaller teeth this could have been avoided for the relevant dimensions. Nonetheless it illustrates that there is a limit to how close to unity the rotor ratio can be before the cog wheels interlock. For the prototype, using a smaller rotor dimension results in a more than halved torque potential. As the PMHRM's main advantage is the torque potential, the interlocking problems give a poorer machine. This mainly the reason that the Steromotor and other prototypes use V-grove surface.[6], [3]

Analysis showed that it was difficult to construct a sensible three-phase winding from the 16-slot machine. Deciding on 16 slots was a mistake, especially if the motor is to run on three phase.

To filter the eccentric, vibrating movement from the rotor shaft, it was decided to use a solution with angular joints and an eccentric double ball bearing support. This was considered a foolproof and sturdy solution, and possible to build more or less from shelf ware. It is not very compact, and for a commercial application where compactness is of importance, another solution should probably be found. On compact alternative is that of the Steromotor.[2]

VII. Further work

The prototype is at the time of writing not completed. Although plans are laid, the shaft bearing solution has not been finalized. To operate the machine as generator a motor must be fitted to drive the input shaft.

Due to problems with the cog-wheels, the current prototype only has a gearing ratio of 1:9. To reveal the torque potential of the machine, efforts should be made to mount a larger rotor in the machine.

So far in the study of the PMHRM only theoretical studies have been conducted. Both of the two simulation models in

their current state leaves a lot to be desired. The magnetic circuit model needs detailing, and the torque calculation method needs verification. If the time dependent FEM-study can be solved it will probably be the better tool. The radial band method mentioned should be investigated.

Although some weaknesses in the design already have been found it is likely that testing will reveal sources of loss and of weaknesses in the proposed assembly. Testing will also verify simulation results. Testing the machine as a generator will be the first step in a testing plan. For motor operation, tests can be performed with three phase. With a converter more opportunities arisle. As discussed the machine seems to perform with a separate phase for each coil, and facilitating such a drive is a challenge.

VIII. Conclusion

Theoretical studies of the PMHRM have been conducted, and based on these a feasible concept has been proposed. A prototype machine has been designed based on the proposed concept. The process of building a PMHRM is well under way. All critical parts are in place, and awaiting assembly. Two models for simulations on the prototype has been built.

Theoretical studies show that the torque potential for the machine type is very high. Controlling the coils individually increases the torque potential from the traditional Steromotor. Torque density to rotor swept volume benefits greatly from a high magnetic field density in the air gap. As more copper and PM volume is needed in the stator to achieve higher field density, torque density to total volume is not increased that much. To utilize the torque potential of the PMHRM-machine, the rotor outer radius should be as close as possible to the stator inner radius. The gearing effect is larger, and a short air gap reduces the need for copper and PM in the stator.

Using PM magnetizing can be good for generator purposes, with no copper losses to magnetize the machine. In motor operation the PM only provides a DC-bias. If the motor is operated with full converter control of the coils/phases, no DC bias is needed and the PMs and their volume unnecessary.

Simulations show that the prototype is quite far from the maximum torque potential, with approx. 6.5% of theoretical torque density maximum. Using cog wheels as mechanical bearings in the machine restricts ratio of rotor to stator radius, and is not an ideal solution. In it's current configuration the prototype will not have an impressing torque. FEM-studies estimate a torque of 72Nm, and a density to rotor volume of $35kN/m^2$. Improving the rotor ratio is crucial to increase it's torque potential, as the stator is not able to produce a large enough field in the current air gap.

Perhaps surprisingly, simulations show that cogging torque is not more than approximately 3Nm at maximum.

IX. Acknowledgements

I would like to thank my supervisor for guiding and motivating me during my work on this project, Oddvar Landrø at the Department Workshop for leading the assembly work and contributing to mechanical solutions, Bjørn Haugen, NTNU for helping with the torque transmission solution, Rune Morten Haug at Smart Motor for help with ordering mechanical parts, Anyuan Chen at SmartMotor for helping me in the process of ordering magnets and stator laminations.

References

[1] R. Schön, "Elektrische Wälzmaschinen", *Elektrotech & Maschinenbau, 1961, 78, pp257-266*

[2] R.A. Aschen, H.R. Bolton, "Aspects of the hypocycloidal reluctance motor", *IEE Proceedings, Vol.128, Pt.B, No.6, November 1981*

[3] J. Reinert, J.H.R. Enslin, E.D. Smith, "Digital Control and Optimization of a Rolling Rotor Switched Reluctance Machine", *IEEE Transactions 1993*

[4] A, Viviani, "Experimental and Theoretical Study of Hypocycloidal Motors With Two-Harmonic Field Windings", *IEEE Transactions, Vol PAS-99, No.1, Jan./Feb. 1980*

[5] Å.K. Nilsen, R. Nilssen, "Investigations into a Flux Switching Hypocycloidal PM Machine", *Specialization Project, NTNU 2010*

[6] A. Arkkio, A. Biernat, B. Bucki, G. Kaminski, A. Niemenmaa, A. Smak, P. Staszewski, "Finite-Element Analysis for a Rolling-Rotor Electrical Machine", *IEEE Transactions, Vol.46, No.8, August 2010*

[7] S. W. Director, "Circuit theory: A computational approach", *John Wiley & Sons, Inc., New York 1975*

[8] D. C. Hanselmann, "Brushless Permanent Magnet Motor Design", *The Writers' Collective, 2003*

APPENDIX A
THE BUILDING PROCESS

When entering the building process, a lot of mechanical issues had to be handled. When the design of rotor and stator were finalized, they had to be compatible with the already chosen solutions for torque transmission, mechanical bearings and housing. To acquire the solutions for the mechanical parts of the machine, expertise outside the department was used. To deliver the electromagnetical parts, companies LCD Lasercut and Neorem Magnets were hired.

A. Stator lamination

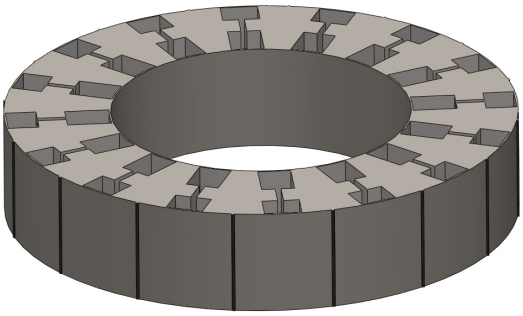

Fig. 14: The stator lamination

Anyuan Chen at SmartMotor, with a PhD from NTNU, has experience from manufacturing prototypes and has been counselling on the process of acquiring the electromagnetic parts for the machine. The stator laminations were ordered from LCD Lasercut in Switzerland. They required a CAD (.dxf) file portraying the stack with correct measurements, along with information of which steel to be used. The stator laminations represent a large cost. To lower the cost of lasercutting, a thickness of 1mm was chosen. The increased hysteresis losses can be justifed with a cost reduction of 655 Euro compared to 0.5mm laminations. As this prototype is not intended used for studies of achievable effectivity-study, loss minimization was not top priority. The designation of the chosen material is M800-100A, from Surhammars Bruk. Grain orientation was considered redundant in this machine as there exist no flux revertion, and the flux travels in multiple directions through the sheets. To keep the stator core together properly together, a welding seam is applied to every section - 16 in total. A circumferencial band of 1 mm is left on the in- and outside of the lamination to hold them together. Magnetically, both these bands should be removed after the stator has been given alternative support. The outer band can prove hard to remove, but will only provide an additional small leakage leg. The .dxf-model was built in SolidWorks.

B. Mechanical bearings

Whether to use cog wheels or friction surface for the mechanical bearings was one of the great uncertainities at the start of the project. Rune Haug at SmartMotor has a wide experience on getting moving parts to move in the right way,

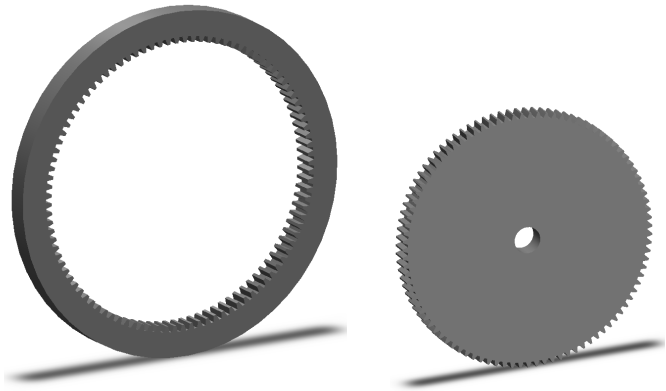

(a) (b)

Fig. 15: a) Outer cog wheel b) Inner cog wheel

and was thus consulted on this matter. It was decided to go for cog wheels, as it gives predictable action and firm frames for the electromagnetic design. Drawbacks are friction losses and need for lubrication. In later stages, switching to friction wheels can be done to lower mechanical losses.

Cog wheels represent a large portion of the costs for the mechanical assembly. The dimension of the cog wheels determines the eccentricity, also for the electromagnetical parts. Eccentricity was then decided by availability of reasonably priced cog wheels. From Jens S. it was possible to order cog wheels from the supplier Mädler. A suitable outer cog wheel had a contact diameter of 200mm (Outer 240mm, inner 196mm) and 100 teeth. Two different inner cog wheels with respectively 90 and 95 teeth, contact diameter 180mm and 190mm, were ordered. The 95 teeth wheel give twice the gearing effect. With concerns of interlocking between the outer wheel and the 95 teeth wheel, the 90 teeth wheel was ordered as a fail proof backup solution.

The backup proved most valuable, as the 95 teeth wheel and the outer wheel were incompatible. Using the 90 teeth wheel, results in a less satisfying magnetical design, and the gearing ratio of the machine is only 1:9, in accordance to eq. 2. The problems with the interlocking could have been solved with smaller gear teeth, but illustrates that there is a limit to how small eccentricity and how large gear ratio you can achieve with cog wheels as mechanical bearings. Existing designs has friction surface or V-grooving.[2], [3].

A switch to plain roller bearings with friction surfaces is recommended if the prototype is to have a high torque potential and lower losses.

C. Torque transmission

As a specialist in the field, Bjørn Haugen of the Department of Engineering Design and Materials at NTNU, was consulted on what basic principle was to be used for torque transmission. For an easy to manufacture prototype of the PMHR-machine, the solution with two angular joints are sufficient. The solution is shown in fig. 16. Due to the prototypes small size and low speed on output shaft, the varying speed of the mid section will not cause significant torque disturbance.

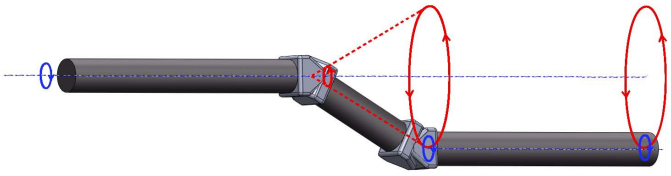

Fig. 16: Illustration of the joint-solution to be used in the machine

The angular joints are a weak link in the torque transmission system. From the Mädler catalogue at Jens-S, article number 631 250 00, was ordered. These are certified for a torque of 240Nm at 200rpm, and 384Nm at 100rpm.

For a larger machine constant velocity joints could be considered to ensure the varying speed of the mid part of the shaft will not cause vibrations and torque pulsations. In wind-turbine applications slide bearings might be more suited as lightning strikes and the following overvoltages might damage the ball bearings.

Ball bearings are needed to support the shaft. To constrict the rotor shaft to it's eccentric path, a solution with one ball bearing eccentrically placed inside another can be used. In the back of the machine a circular groove can be used serve as a slide bearing. These bearings will be able to absorb axial forces to a certain degree. No bearings are yet acquired.

D. Permanent magnets

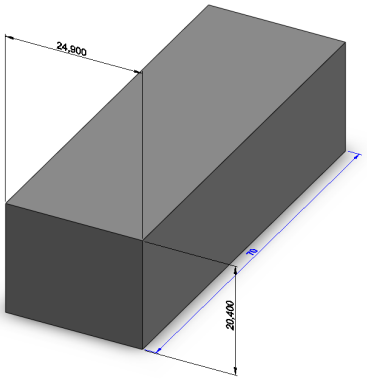

Fig. 17: A single magnet, as ordered from Neorem

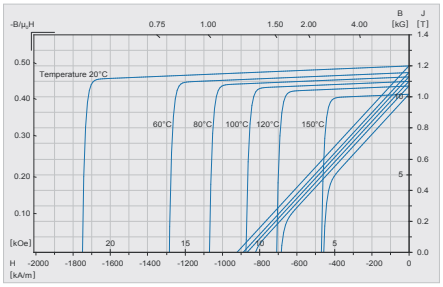

B_r	1.20 T	12.0 kG
${}_BH_c$	920 kA/m	11.6 kOe
${}_JH_c$	1750 kA/m	22.0 kOe
$(BH)_{max}$	270 kJ/m³	34 MGOe

Nominal values at 20°C

B_r	1.15 T	11.5 kG
${}_BH_c$	850 kA/m	10.7 kOe
${}_JH_c$	1550 kA/m	19.5 kOe
$(BH)_{max}$	250 kJ/m³	31 MGOe

Minimum values at 20°C

Fig. 18: The magnetic characteristics of Neorem 476a

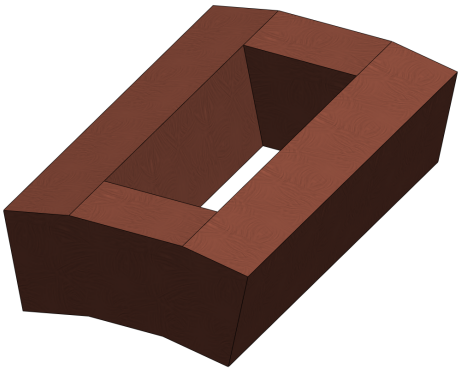

Fig. 19: A single coil

Magnets were ordered through the finnish manufacturer Neorem Magnets. They have been delivering magnets on specifications in earlier NTNU-projects. The magnets are of sintered NdFB, Neorem's type 476a, of a design shown in fig. 17, magnetized in the horisontal direction. A quantity of 20 was ordered, four more than required to allow some assembly mishaps. The magnetic characteristics of the magnet are shown in fig. 18. A tolerance margin to the gaps in the stator lamination of 0.1mm was given to ensure a quick installation.

E. Coils

The coils were designed to fill the slots with some margins. Winding the coil with $1.3mm^2$ wire should allow more than 300 turns. According workshop tables for grouped conductors, a RMS current of 10 ampere will not make the winding temperature exceed 100 degrees. Thermal studies of the windings under steady operation have not been conducted. Fig. 19 shows a rough sketch of the coil.

F. Rotor laminations

The rotor is to be made at the workshop to match the inner cog wheel. It's outer dimension is 179mm, allowing for a minium airgap of 0.5mm in the machine. To save weight it is made hollow. The lamination thickness is 0.5mm.

G. Assembly

The assembly of the machine is done by the workshop of the Department of Electric Power Engineering at NTNU, with Oddvar Landrø in charge. He has also contributed a lot to the design of the mechanical solutions.

To give room for the coils, spacers are needed between the stator laminations and the outer cog wheel. Adding spacers in the stator calls for spacers in the rotor assembly, as the cog wheels have to be aligned. The spacers will be torque carrying and radial forces will follow the contact point. Under-dimensioning must be avoided. It is important that the spacers, especially the stator spacers, are of a non-magnetic material.

The stator consists of almost separate units, only a 1mm thick band on the outside circumferenc holds them together as the inner band is removed. Extra mechanical support is

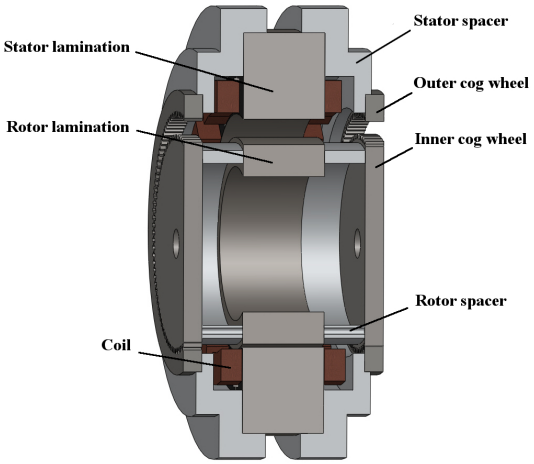

Fig. 20: Cross section view of machine

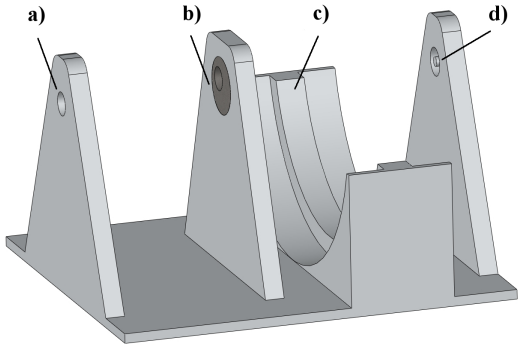

Fig. 21: Machine frame

required in the stator to withstand the forces it will be subjected to. A non magnetic material is inserted to the leakage gaps in the stator, and the stator spacers are designed to support the stator. Fig. 20 shows a possible stator assembly. The figure shows a suggested design of spacers, these are likely to be modified.

A proper frame is needed to assemble the machine from the individual parts. The functionality of the different parts of the frame in fig. 21 are as follows:
a) Bearings for the output shaft.
b) Eccentric bearings in the front of the machine restricts the rotor to an eccentric path as discussed in sec. A-C. They can also absorb limited axial forces.
c) Slide bearing erving the same purpose as the eccentric bearings, and can absorb large axial forces.
d) Support for the stator.

H. Interchangeable rotors

It would be interesting to test a PMHRM with a larger rotor than the current one, giving higher torque and gearing ratio. To keep costs down, only the necessary parts should be replaced to fit the larger rotor. These parts are rotor laminations, rotor cog wheels/bearings, the eccentric bearings in front of the machine and the shaft between the angular joints. Depending on the new rotor, stator bearings may be exhcanged, and the stator spacers modified. This means that a reversible mounting/fastening is preferred to glue in the interfaces between the interchangeable parts (Rotor, rolling surface, eccentric bearings) and the reusable parts (The stator assembly and rig).

APPENDIX B
THE MAGNETIC MODEL

This appendix aims to establish a model for analyzing the HRPM-machine, and how different control schemes and machine parameters influence it's perfomances. Comparative calculations of voltage and torque potential have been conducted for the two rotor dimensions of interest in the prototype. Only results with the 189mm rotor are illustrated with graphs. The matlab-script created (found in app. D and in digital form through the ENO-group at Department of Electric Power Engineering) allows adjustment to several more parameters.

A. Modeling the HRPM-machine

This section intends to establish a magnetic model as a basis for dynamic simulations of the machine. Finding the flux linkage is used as a starting point to find induced voltage, and the machine torque through the co-energy method.

$$\underline{\lambda} = \underline{LI} \tag{14}$$

To determine the inductances of the machine, the magnetic circuit equivalent in fig. 22 is used. While the leakage-leg and PM-reluctances are equal around the machine, the air-gap reluctances are different from eachother and dependent on the rotor position. Air gaps lengths are approximated to the minimum gap in addition to a sinusoidal component of amplitude equal to the eccentricity. This is a simplification generally used in the study of this machine [2], and it holds true as long as k_r and r_s are fairly equal. The iron reluctance is considered negligible. Zero slot leakage flux is assumed. These reluctances can easily be added, if necessary.

The magnetic equivalent of fig. 22 may be reworked to a better schematic, and more generic version as in fig. 23. From there, the leakage gap and magnet gap relutances ($\Re_l, \Re_m$) are gathered in a single parameter, $\Re_s$.

The values of the different parameters are given by the specification and dimensions of the prototype. Some approximations and assumptions have been made. The magnetic circuit only allows lumped parameters and the air gap length is constant for each air gap. Splitting the air gap into several parallells could have made it more realistic.

Effective area of the air and leakage gap is larger than the iron cross section. The leakage gap has a fringe contribution to permeance given by the following formula [8]:

$$P_f = \int_0^X \frac{\mu_0 l}{g + \pi x} dx = \frac{\mu_0 l}{\pi} ln\left(1 + \frac{\pi X}{g}\right) \tag{15}$$

where l is length of the machine, g the leakage gap length, and X is the distance the field creeps up the iron on each side of the airgap. The Carter coefficient for the stator to rotor air gap can be expressed as

$$k_c = \left[1 - \frac{\omega_s}{\tau_s} + \frac{4g}{\pi\tau_s} ln\left(1 + \frac{\pi\omega_s}{4g}\right)\right]^{-1} \tag{16}$$

where ω_s is the width of the slots, τ_s the width of a slot and a tooth and g is the air gap length. This factor is to be applied to the gap length, and the area is equal to the slot and tooth area. With the varying air gap length, the coefficient varies from 2.23 at the smallest air gap, to 1.26 at he largest. The factor is set at constant 1.8 in the script for this analysis, but could have been implemented as a posititon dependent variable with some effort.

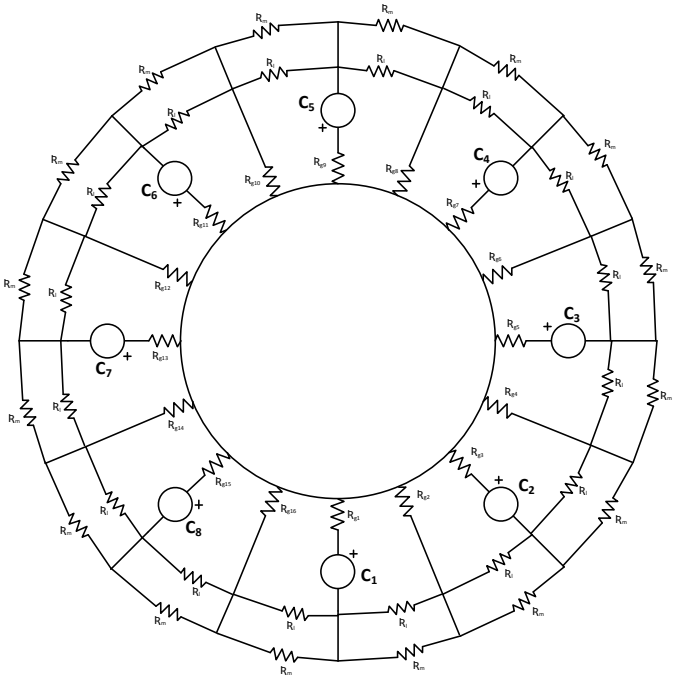

Fig. 22: Magnetic equivalent of the HRPM-machine, without the PM contribution

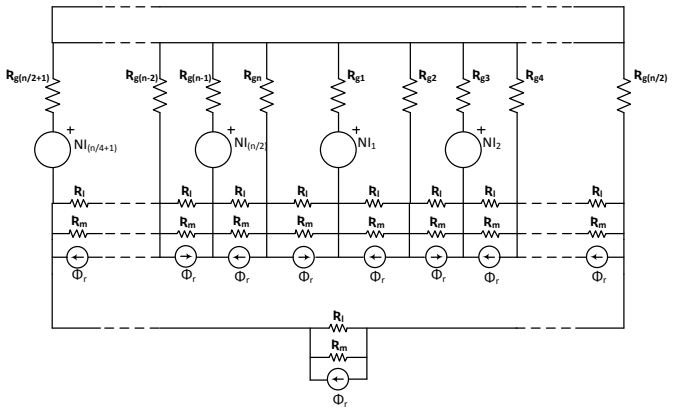

Fig. 23: Generic equivalent of the HRPM-machine, a single coil superpositioned.

B. Analytical approach to inductances

From traditional magnetic circuit analysis the inductances in the machine can be expressed as a function of circuit reluctances, turns in coil and remanence in the magnets. Eq. 17 is an expression for self inductance of coil i.

$$L_{ii} = \frac{N_1^2}{\Re_{gi} + \Re_m} \tag{17}$$

R_{gi} is the air gap reluctance in the air gap from the top of coil i and to the rotor, while R_m is the reluctance from the

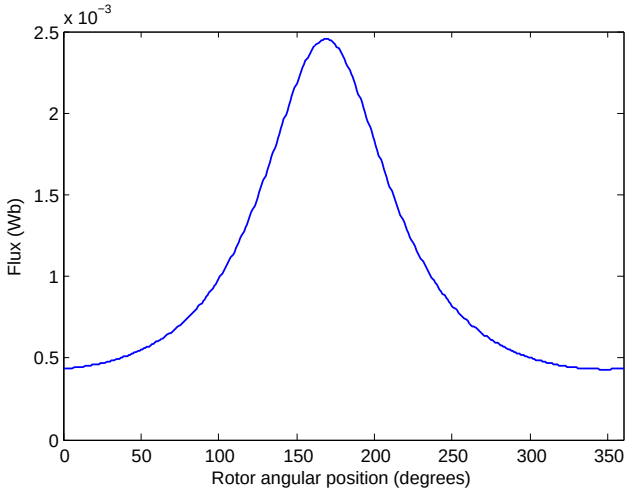

Fig. 24: Flux linking from PMs to coil, analytical approach

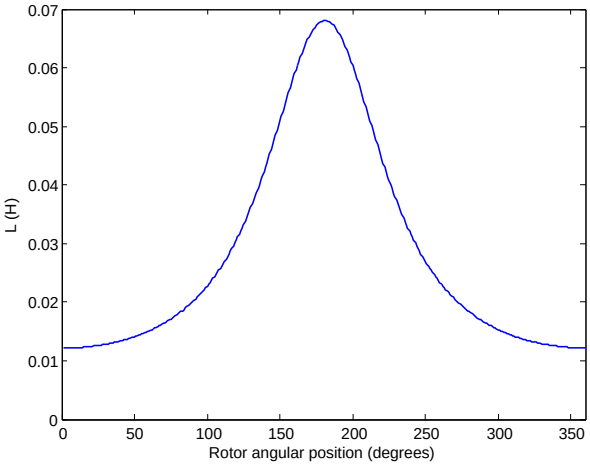

Fig. 25: Self inductance of one coil with respect to rotor position

rotor back to the bottom of the coil leg i - not including the path through R_{gi}

The mutual inductance between two coils is expressed by eq. 19

$$L_{ij} = \frac{N_i N_j \Re_m}{\Re_{tot}(\Re_m + \Re_{gi})} \tag{18}$$

an expression more specific for the HRPM-machine can be deducted.

$$L_{ij} = \frac{N_i N_j \Re_m}{\Re_m(\Re_{gi} + \Re_j) + \Re_{gi}\Re_j} \tag{19}$$

Where $\Re_m$ is the reluctance of all paths not leading through coil i or j, $\Re_j$ is the reluctance of the path from the rotor through coil j. Looking at the equivalent in fig. 23, it becomes obvious that $\Re_m$ is difficult to find with a traditional approach. Simplifications are needed. Which parts to omit varies with the rotor position, and makes it hard to do simplifications without significant impact on the result.

It is possible to provide a reasonable simplification for the flux linkage from the PMs to the coils. With the leakage gap dominating when air gap to rotor is large, one stator actuator unit may be considered as a separate system.

$$\begin{aligned} \lambda &= N\Phi_m \frac{\Re_{leak}}{\Re_{leak} + \Re_{gap}} \\ &= N\Phi_r \frac{l_m l_{leak}}{(l_m + \frac{2l_{gap}l_{leak}}{2l_{gap}+l_{leak}})(2l_{gap} + l_{leak})} \end{aligned} \tag{20}$$

The expression in eq. 20 it's assumed that air gap to and from rotor is equal. This is valid for a machine with a very large number of actuators, but not quite for the prototype with only 16 teeth. The flux linkage is proportional to the flux density drawn in figure 24

C. Node reluctance approach to inductances

To further investigate the inductances, especially the mutual inductance, an approach known from electric circuits is used. Describing power systems and other large electric circuits can be done by arranging the whole grid in an impedance matrix.[7]. Building on a core by PhD Svein Magne Hellesø and Prof. Hans Kristian Høydalen, a script is written that adapts the concept to magnetic circuit equivalents.[8] For a magnetic circuit the following relation, analogous to Ohm's law in electric circuit, is valid

$$\underline{MMF} = \underline{\Re} \cdot \underline{\Phi} \tag{21}$$

The $\Re$ matrix contains the reluctance between any two nodes in the magnetic circuit, while the MMF and Φ-matrices contains the voltage in and net flux through every node in the system. From this relation a lot of values can be extracted. This node reluctance method is an alternative to FEM-analysis. Approximations are necessary and errors more significant in this model than in a FEM-program, but it is a powerful and easy tool to use if limits on accuracy are kept in mind. The Matlab script is found at the back of the appendices.D

By extracting the node to ground reluctance from the reluctance matrix set up with the matlab-script, the self inductance can be found with the following equation:

$$L_i = \frac{N_i^2}{\Re_{eq}} \tag{22}$$

The result is drawn in fig. 25

To find the flux linkage between a coil and the PMs, the magnets are superpositioned as the only source of magnetism, and eq. 23 is used.

$$\Phi_m = \frac{MMF_{gi}}{\Re_{gi}} \tag{23}$$

In contrary to the analytical approach all magnets and the different air gap lengths are included in the calculations. Fig. 26 shows Φ_m as a function of rotor position. Comparing this to the results of the directly analytical graph of fig. 24 shows much similarity, this verifies that the nodal-reluctance model is working satisfactory to this point.

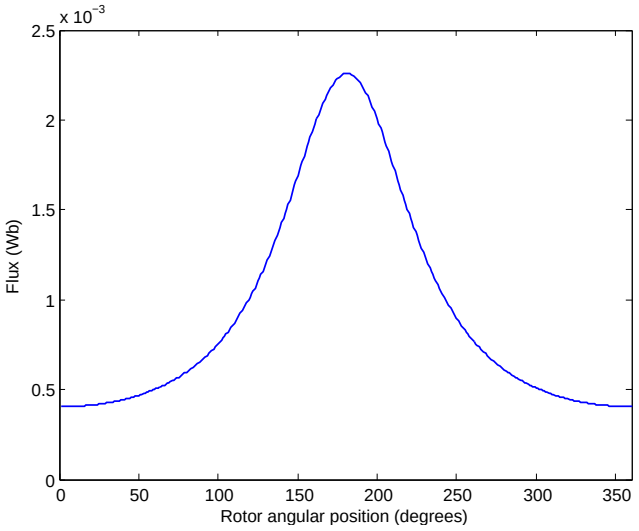

Fig. 26: The flux from PMs linking to coil, nodal approach

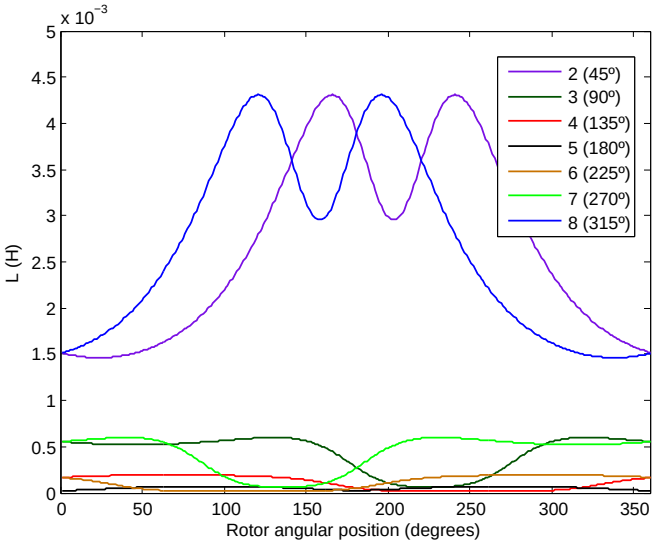

Fig. 27: Mutual inductance between a coil (no.1) and other coils in the machine. Angular displacement of coils indicated

For the mutual inductance, a single coil is superpositioned in the grid. Then the flux through the other coils is found by the following relation

$$\Phi_{ij} = \frac{MMF_{gj}}{\Re_{gj}} = \frac{MMF_r - MMF_j}{\Re_{gj}} \tag{24}$$

where MMF_r is the magnetomotoric potential in the rotor, and MMF_j is the potential at the given coil. R_{gj} is the reluctance of the air gap at the given coil. The mutual inductance is then found by equation 25

$$L_{ij} = \frac{N_j * \Phi_{ij}}{I_i} \tag{25}$$

Fig. 27 shows the different mutual inductances, and the relations between them. The mutual inductances are depending on the angular distance between the coils, and the position of the rotor. The contribution from the neighbouring coils dominate, as both the relating air gaps are small simultaneously. As shown more detailed in fig 28, the inductance of two coils equally displaced from the reference coil are equal in amplitude and shape, but are time shifted equal to their physical displacement.

Simulations with alternative HRPM-machine parameters show that the shape of mutual inductances varies greatly with the ratio between reluctances in leakage gap and air gap. Compared to self inductance and linkage to the PMs, mutual inductance between different coils is marginal.

D. Induced voltage

The induced voltage in each coil can be found through the following expression,

$$e = \frac{d\Phi}{dt} = \frac{d\Phi}{d\Theta}\frac{d\Theta}{dt} \tag{26}$$

Where Φ is the flux flowing through the coil. Only considering the contribution from the permanent magnets, the induced voltage can be found with the node model. Fig. 29 shows the induced voltage in a single coil. Notice that the induced voltage is at the most active when the air gap between coil and rotor is close to minimum. When the rotor is on the opposite half of the stator, the voltage is at rest.

Specifically for the prototype, it is difficult to create three symmetrical phases from eight coils or 16 slots. In general the nonsinusoidal shape of the voltage from each coil makes it contraproductive to build phase voltages from the machine by series connected coils. Shown in fig. 30a, the voltages from different coils will oppose each other in when they are at peak. This makes the peak voltage of a phase built from two coil just 37% larger than the single coil contribution. Further, creating a phase from four coils gives only a further increase of 10.8% in amplitude. The voltage RMS when series connecting four coils is only increased by 97% compared to the voltage RMS of a single coil.

TABLE V: Voltages induced at $\omega_{mech} = 63rpm$

	V_{peak}	V_{RMS}
Single coil	59.4	20.6
Two coil phase	81.4	33.3
Four coil phase	90.2	40.6

These numbers, if not totally unacceptable, indicates that the nature of the machine causes great losses in efficiency and voltage and power density when operated as a three phase generator. The peculiar shape of the voltage also indicates that a large amount the most energy efficient operation of the machine gives/requires a current of the same peculiar shape. Using more standard current schemes, as in cpt. B-E, requires reactive power.

E. Finding torque potential through co-energy

The theoretical background of this section is taken from chpt. 3 and 4 in Hanselmann 2003 [8].

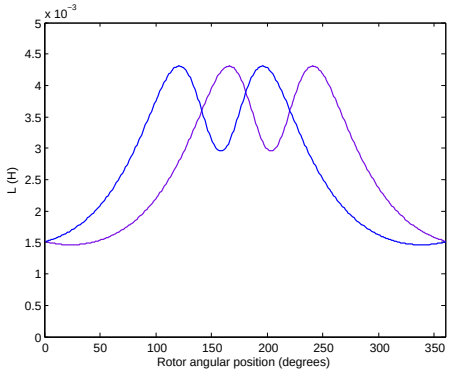

(a)

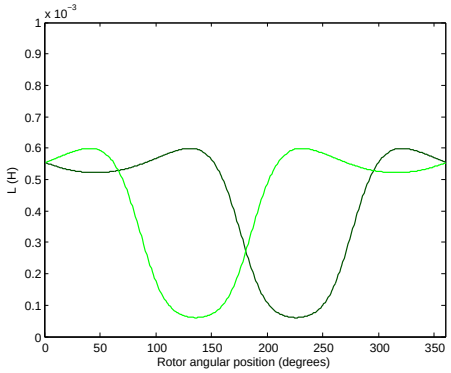

(b)

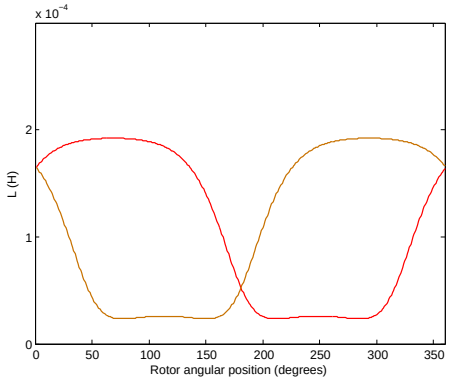

(c)

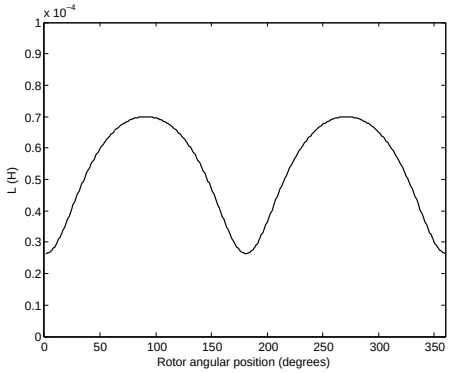

(d)

Fig. 28: a) Coils displaced 45^o b) Coils displaced 90^o c) Coils displaced 135^o d) Coil opposite

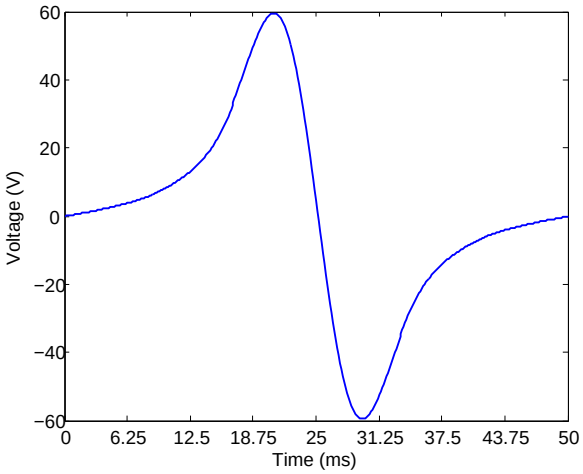

Fig. 29: Voltage induced in a single coil due to PM-flux

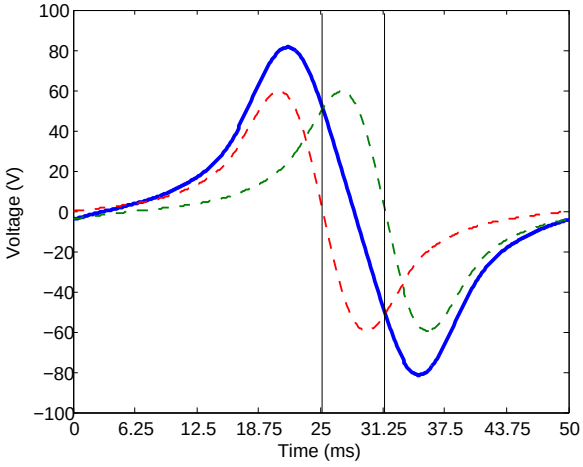

(a)

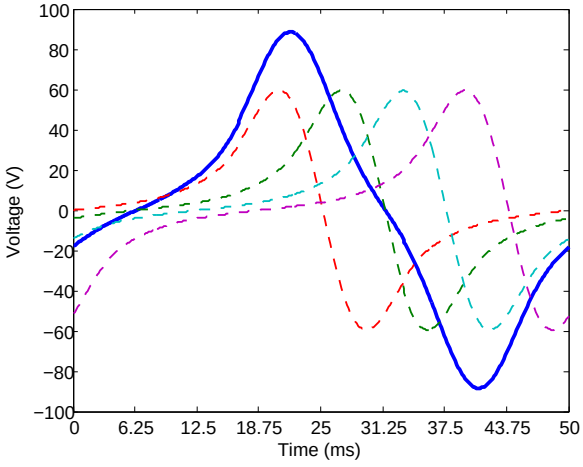

(b)

Fig. 30: Phase voltage: a) from two coils b) from four coils

A way to find torque is in the rate of change in the mechanical energy of the machine

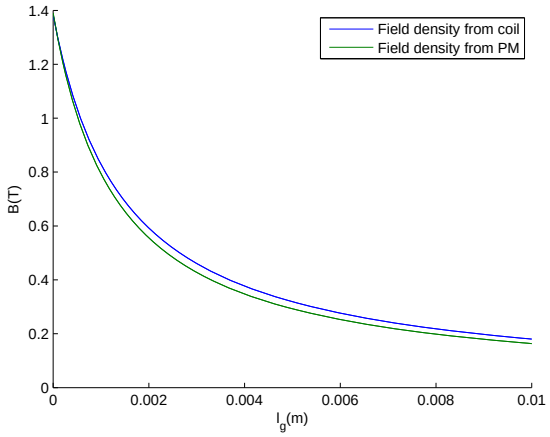

Fig. 31: Flux through air gap from coil and magnet at increasing gap length, rated current and constant stator parameters

$$T = \frac{dW_m}{d\Theta} \tag{27}$$

The rate of change in the mechanichal energy is proportinal to the rate of change in magnetic energy in the machine. Co-energy is a fictional quantity equal to energy, for a standard PM-circuit it can be expressed as,

$$W_c = 1/2Li^2 + 1/2\Re\phi_m^2 + Ni\phi_m \tag{28}$$

where ϕ_m is the flux from the magnet linking to the coil. The mutual term between different coils is left out of the expression, but included in the calculations. This was assumed to hold true for the PMHRM too, but this as falsified by weird results in simulations. By investigation it was found that the expression eq. 28 only considers the reluctance seen from the magnet through Φ_m extracted from the node-reluctance matrix. Since the reluctance seen the from coil is rather different, the coil's ability to induce an opposing flux, and thereby torque, is not considered by eq. 28. It seems something is lost in the translations from energy to coenergy.

While deriving a correct analytical expression for the co-energy proved to much for the author, an effort is made to approximate an expression; a (dubious) scaling factor is introduced. The scaling factor is based on simulation empirics and the coil's ability to create flux. As shown in fig. 31 the flux ability is equal to that of the PM with the standard stator specifications. Increasing the leakage gap also reduces the coil's ability to create flux. The scaling factor is then:

$$K_{s1} = \frac{\Re_g + \Re_{s(standard)}}{\Re_g + \Re_{s(actual)}} \tag{29}$$

If no alterations are done to the stator, the scaling factor is unity. Altering the stator design is hypothetical, but a theoretical case is used to quantify the benefits from the leakage gap design.

$$W_c = 1/2Li^2 + 1/2\Re\phi_m^2 + Ni\phi_m K_{s1} \tag{30}$$

If all mechanical losses are modelled externally of the motor, equations 27 and 30 can be combined to a torque expression.

$$T = \frac{dW_c}{d\Theta} = \frac{1}{2}i^2\frac{dL}{d\Theta} - \frac{1}{2}\phi_m^2\frac{d\Re}{d\Theta} + Ni\frac{d(\phi_m K_{s1})}{d\Theta} \tag{31}$$

The different values for inductance, reluctance and flux can be found with the node reluctance model. There is one limitation though, every change is a time step, and the torque may then only be estimated by

$$T = \frac{dW_c}{d\Theta} \approx \frac{1}{2}i^2\frac{\Delta.L}{\Delta\Theta} - \frac{1}{2}\phi_m^2\frac{\Delta\Re}{\Delta\Theta} + Ni\frac{\Delta(\phi_m K_{s1})}{\Delta\Theta} \tag{32}$$

With eq.32 the torque potential for the machine torque potential of the machine was investigated under different current schemes.

It is also important to be aware that the magnetic reluctance model implemented in Matlab only observes the oscillatory movement of the rotor around the stator axis, and the $d\Theta$ in eq.31 is referring to this movement. To read the torque potential on the rotor axis, the results derived from the model are scaled by the gearing ratio, 19:1 or 9:1 for the prototype machine depending on rotor diameter.

F. Doubts around the torque expression

In a standard motor, the only substantial airgap is the main gap between rotor and stator, but in the PMRHM the leakage gap is of same magnitude. The error might be that energy exchanged with in the leakage leg is included in the torque expression when it is not contributing to torque. The leakage gap don't move net energy to and from the leakage gap is zero, the term $Ni\Phi_m$ does not necessarily reflect this, as the current varies. If these suspicions are correct, another scaling factor should be used. The factor eliminates the energy in the leakage gap from the equation and is defined as in eq.33.

$$K_{s2} = 1 - \frac{\Re_l}{\Re_g + \Re_{s2}} \tag{33}$$

Testing or more theoretical studies should be done, and K_{s2} might very well prove the better scaling factor.

An alternative way is to use the script to find the flux through each airgap and then calculate the forces and torque from those values.

G. Torque with different currents

Calculations are run for different current control schemes. In short, the four different current schemes are as following.
1. Constant current, a constant current is flowing through all coils at all times.
2. Individual control, rated current are given to coils within 90 degrees in advance of the rotor. Negative rated current is applied to coils within 90 degrees behind the rotor.
3. Three phase, regular three phase operation.
4. Eight phase, all coils have an sinusoidal current.

No current scheme is optimized to the machines natural voltage (See sec.B-D, and usage/production of reactive power will probably be considerable. A summary of the results is presented in table VI.

From eq. 31, the torque contribution from a single actuator unit can be divided in to four different components;
from self inductance, $0.5 * i_i^2 \frac{dL_i}{d\Theta}$,
from mutual inductance, $0.5 * i_i i_j \frac{dL_{ij}}{d\Theta}$,
from PM linkage, $N_i i_i \frac{d(\phi_m K_{s1})}{d\Theta}$,
and the PM reluctance (cogging) torque, $0.5 * \phi_m^2 \frac{d\Re}{d\Theta}$.

In the matlab script these components were calculated and summed for each coil, and then the sum of the contributions from each coil were added to retrieve the total torque in the machine.

1. The first calculations are done with constant rated current in the coils. As the field is approximately equal on both sides of the rotor (refer to fig. 1), forces from the different sectors levels each other out and only cogging torque at certain positions remain. Torque as a function of rotor position is shown in fig. 32.

As can be seen in fig. 32c the average torque found in simulations is not exactly zero. This bias is discussed in section B-I

2. The second set is run with individually controlled coils. The coils are activated when the rotor is 90 degrees from the coil, and deactivated when the rotor is at the coil. This will cause creation of force pulling in the positive direction. Behind the rotor, negative current is applied to the coils to neutralize the field from the PMs and reduce the forces pulling the rotor in negative direction. [5] If the coil is to be activated earlier than 90 degrees, a component of the force will reduce the normal force necessary for friction. See fig. 1. The current is set to positive or negative rated value for the 90-degree intervals, and zero everywhere else. Turning the current in a coil on and off instantaneously is not possible, even though the electric time constants are small, transients will be created. This simulation should only be regarded as rough sketch for the torque obtainable under individual control operation of the machine.

Fig. 33 shows the different torque components in

a single unit. Fig. 34 show total torque contributions for each coil, and the total torque for the machine.

The graphs show that the flux linkage and self inductance are the main contributors to the total torque. Also the cogging torque from a single unit is considerable, but in the total picture the different units balance each others cogging torque.

3. Regular three phase is investigated in the third set of calculations. A challenge is that the prototype does not have a mulitple of three as a slot number, in retrospective a design error. Two coils will have to be split between two phases. Referring to fig. 22, phase A is given coil 1, 2 and 2/3 of coil 3. Phase B has 1/3 of coil 3, coil 4, coil 5 and 1/3 of coil 6. Phase C has 2/3 of coil 6 and coil 7 and 8.

Another issue with sinusoidal current is how much the current should lead the rotor. As discussed in sec. II this will affect the torque potential and the copper losses. The leading angle is defined from the current in coil 1. If phase A reaches

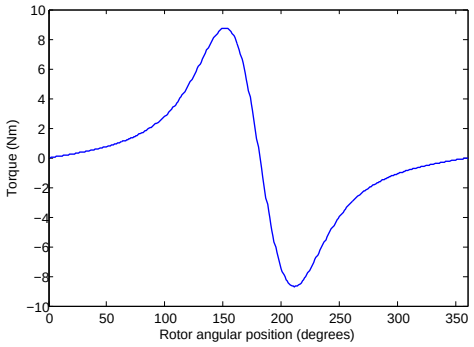

(a)

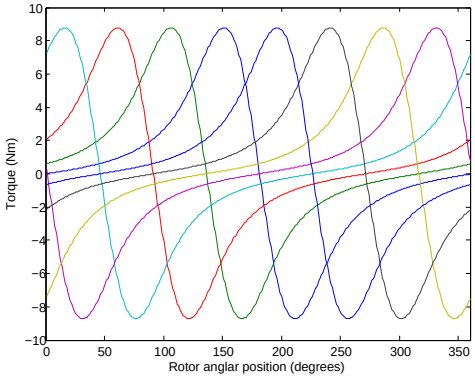

(b)

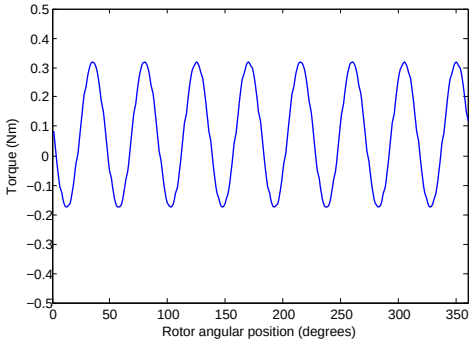

(c)

Fig. 32: Constant current: a) Torque from coil 1 b) Contributions from each coil c) Total torque

maximum when the air gap is at minimum at coil 1, the lead angle is zero. The leading angle giving the largest torque was found to be around 38 degrees.

As fig. 35 shows, symmetry is not obtained and ripple through one rotor revolution is very large, around 200 Nm peak to peak. It reaches it's maximum 222 Nm at a leading angle of approx. 15 degrees.

Although the torque available through three-phase operation is decent, the option is ruled out by a very high torque ripple, leading to vibrations and wear. Before leaving the three-phase approach entirely, more investigations into alternative winding layout should be done. Also for a different machine where phase windings can be laid symmetrically laid out, three phase operation will probably be a reasonable alternative.

4. A fourth set of calcuations is carried out with individual

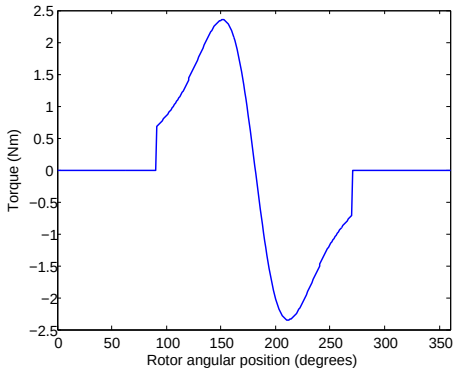

(a)

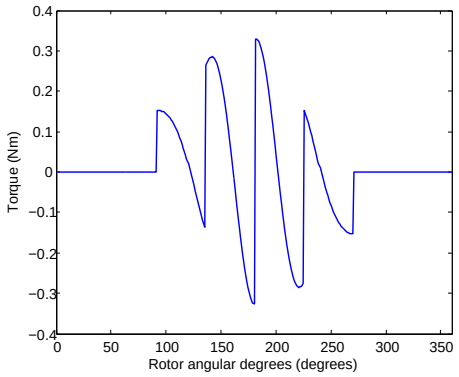

(b)

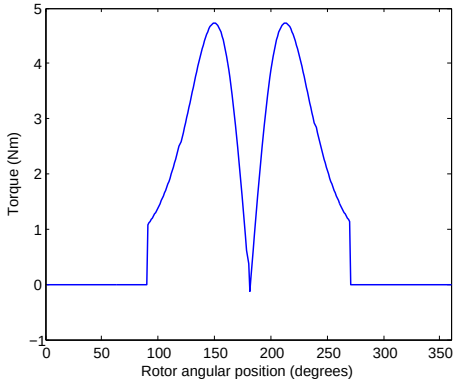

(c)

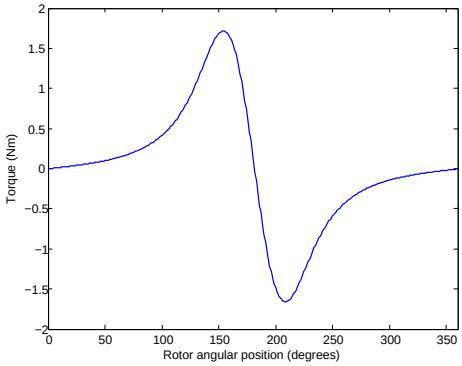

(d)

Fig. 33: Ind. control: Torque contributions from: a) Self inductance b) Mutual inductance c) PM linkage d) PM Reluctance

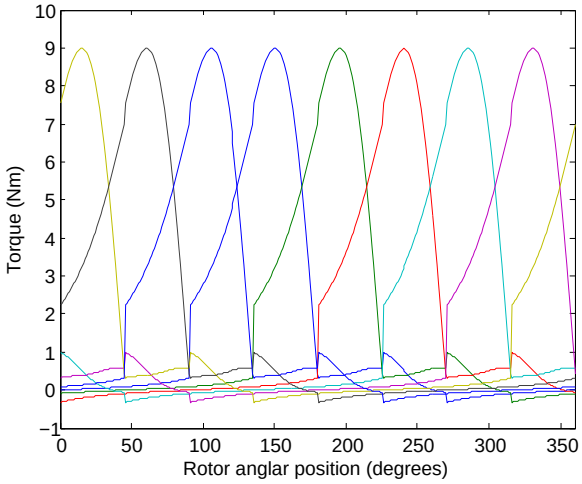

(a)

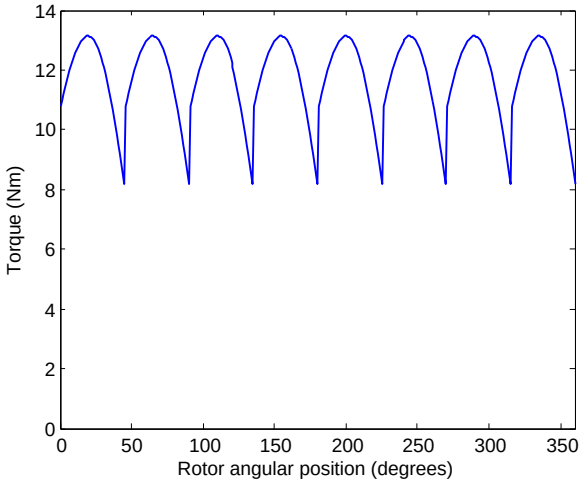

(b)

Fig. 34: Ind. control: a) Torque contributions from each coil b) Total torque

sinusoidal current in each coil (8-phase). Connected to a regular grid, a DC - link converter creating 8-phase sinusoidal current will be more advanced than a pure square signal converter.

Again leading angle is defined as the lead of the current maximum to the air gap minumum. The ideal lead angle for torque is found at 70 degrees. The peak to peak ripple was found to be largest at 0 degrees leading angle, from there it decreases through the area of interest. As fig. 36a shows, with individual control the torque contributions are again symmetric. Compared to case 2, the ripple is lower. Fig. 37 is included for a graphic understanding of the torque, and for comparison with fig. 33.

The 8 phase current scheme is by far best when it comes to torque ripple.

H. Effect of the leakage gaps

The main purpose of the leakage gaps is to provide the coils with the ability to create a magnetic field and thereby

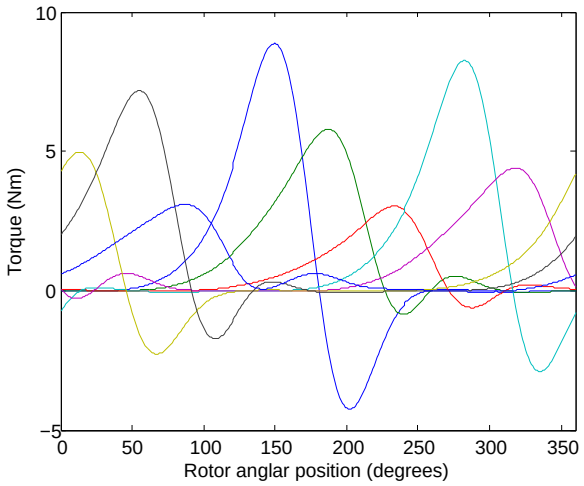

(a)

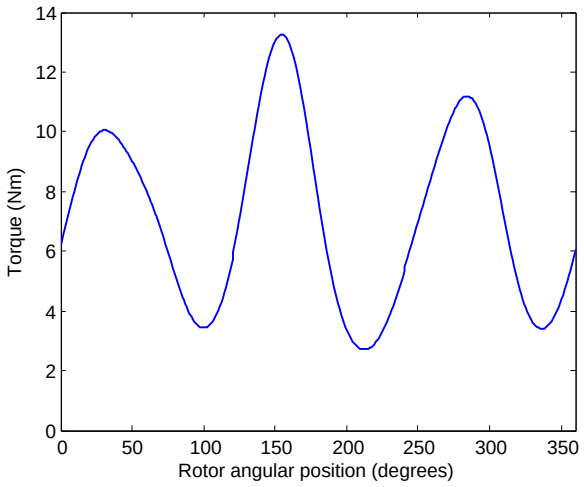

(b)

Fig. 35: 3-Phase a) Torque contributions from each coil b) Total torque

TABLE VI: Torque potential of the prototype under different control schemes and rotors

Current operation	**Torque (Nm)**		**Ripple (Nm)**	
Rotor:	*189mm*	*179mm*	*189mm*	*179mm*
Constant current	1	1	9.4	20.7
Individual control	223	111	60.3	88.8
3-phase	136	59	200.5	111.2
8-phase	174	77	7.9	12.4

unbalanced electromagnetical forces on the rotor. In addition they are a flux weakening feature. The ccost is that slightly more PM volume is needed as some of the PM flux is diverted from the coil to the leakage gap, reducing the induced voltage.

To investigate alterations of the stator design, the scaling factor mentioned (eq. 29) was implemented in the matlab-script. Two torque calculations without a leakage leg were conducted and compared with the corresponding results with leakage leg included.

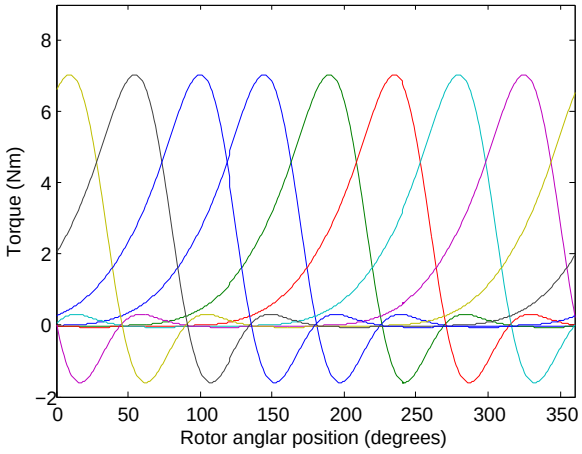

(a)

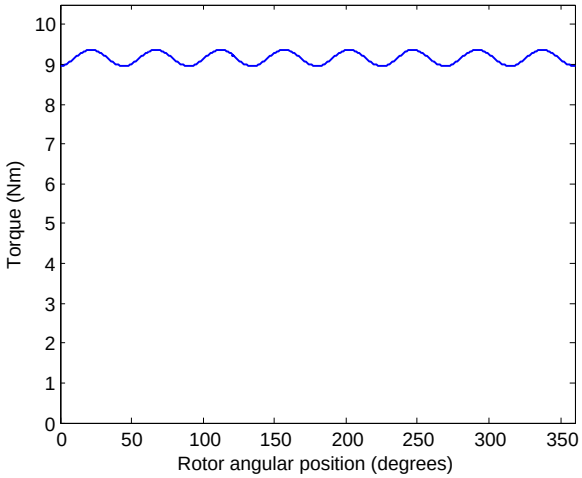

(b)

Fig. 36: 8-phase: a) Contributions from each coil b) Total torque

TABLE VII: Torque with and without leakage legs

	Torque (Nm)		**Difference (%)**
Control scheme	*Leakage path*	*No leakage path*	
Individual control	223	16	-93
8-phase	174	29	-83

Even if the scaling factor is not to be trusted entirely, the numbers are clear enough. In accordance with theoretical assumptions a leakage path is required in a PMHRM-design for the machine to give torque.

I. Weaknesses in the node reluctance script

By studying the results for cogging torque, it becomes apparent that the node reluctance script is not accurate. Fig. 38 shows a net positive cogging torque - which indicates a perpetuum mobile. It can be small deviances accumulating. It can also be a numerical error in the torque-script, as it seems to be a constant error bias.

From the modelling of the machine, many approximations were made. To give accurate results, the air gaps can be

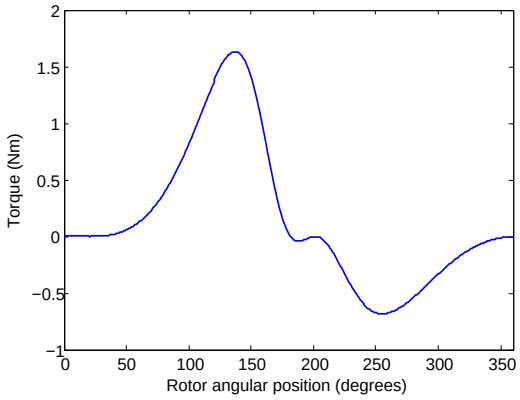

(a)

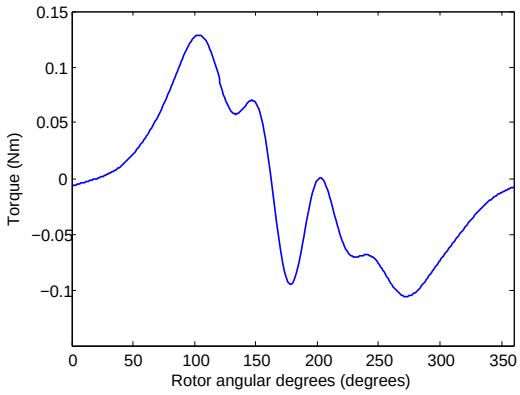

(b)

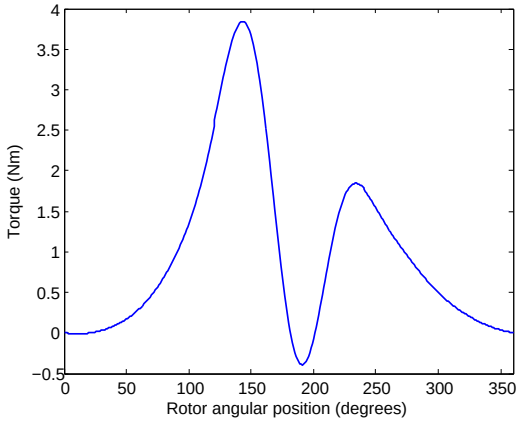

(c)

Fig. 37: 8-phase, torque contributions from: a) Self inductance b) Mutual inductance c) PM linkage

modelled in the better way and the iron reluctances should be included.

In general, the numbers found by calculations in the sections above should not be regarded as 100% accurate.

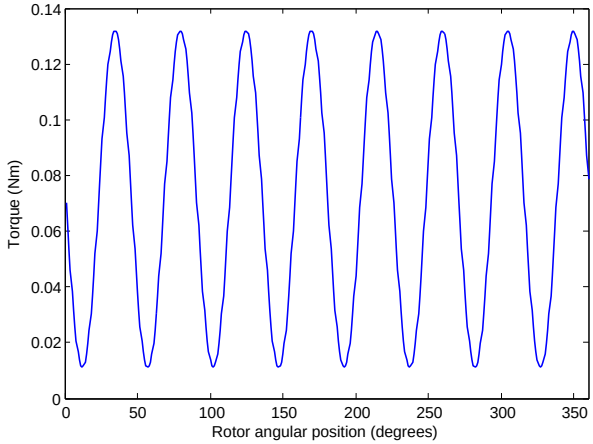

Fig. 38: The total cogging torque with individually controlled coils

APPENDIX C
COMSOL MODEL

A 2D model similar to the prototype machine was built in Comsol, using the 'Rotating Machinery'-module. Due to the rotor's eccentricity, the whole machine cross section had to be modelled. The model is time consuming to solve on a standard laptop, mainly to due to the material's nonlinearity, some narrow air gaps and sharp edges. Some approximations were made to shorten the solving time of the model.

Both a version with the 189mm rotor and one with the 179mm rotor were built. The Comsol model's should be available through the ENO-group at NTNU.

A. Materials

Data for the HB-curve of the stator iron, Sura M800-100A, was collected from the producer's web page, www.sura.se, and included in the model. For the copper and air, the standard library versions were used. PM-regions were approximated as magnetized air (no losses).

B. Geometry

To simplify the mesh, design tolerance margins are not included and the PMs fills the whole magnet space. The stator teeth were filleted to avoid clearly erroneus deviations in the tooth corners.

C. Physics

Permanent magnets were set up with Ampere's law, with remanent flux density in tangential direction as the constitutive relation for the magnetic field. To account for saturation, the HB-curved constituted the magnetic field of the iron parts. The air was constituted by μ_0. Each slot was defined as a multi-turn coil domain, with standard copper conductivity and 300 turns. The slots were coupled in pairs with their neighbour to reflect the physical windings.

D. The stationary analysis

The stationary analysis had two objectives. **1.** To give a good image of the field distribution in the machine with the rotor in different positions. **2.** To give a torque estimate comparable to the values found through the magnetic model-script.

1. Field distribution was found with only the PM-magnetizing the motor. As fig. 39a shows, the machine was far from saturation in that case. Another study was run for a maximum field situation. (Coil 1, 2 and 3 are enhancing the field, while 7 and 8 are pacifies it.) Showed in fig. 39b, this scenario reveals that the leg located at $\Theta = 0$ is heavily saturated (B $>$ 2.3T). Field leaks into the coil domain, but only in the upper corners and the highest value is approx. 0.4T. One should also notice that in the pacified units, the field in the magnet close to the leakage-gap is reduced to a size of approx. 0.5T. According to the magnet characteristics (found in sec. A-D) this is close to the demagnetization point for a temperature of 150 degrees.

A fancy animated GIF showing the field distribution can be found in the digital project folder through the ENO-group.

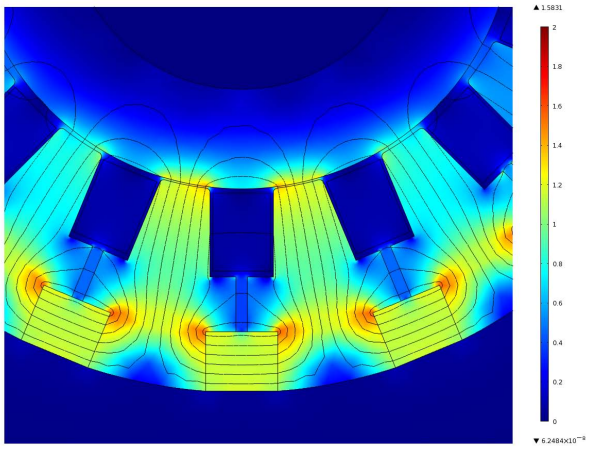

(a)

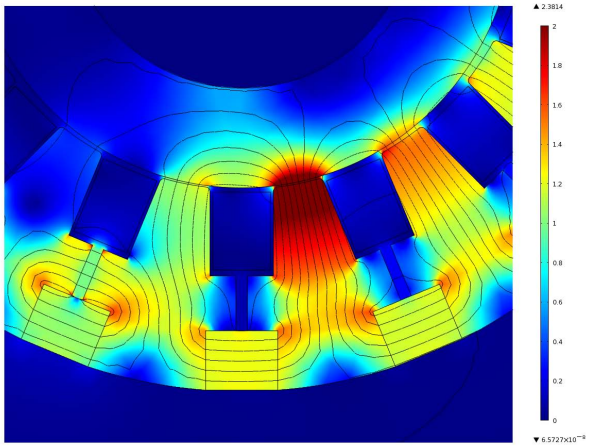

(b)

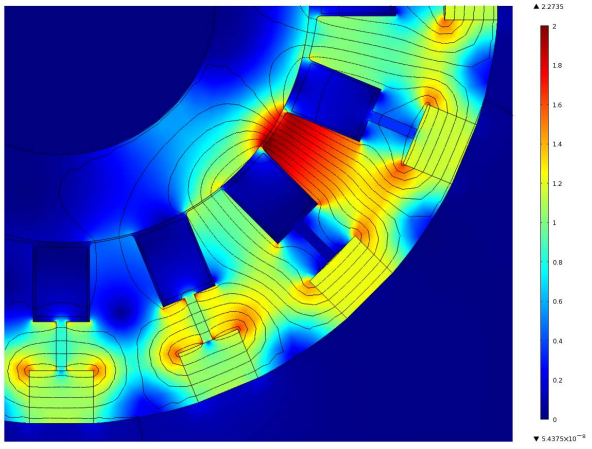

(c)

Fig. 39: a) Only PM magnetization b) Coil enhancing unit c) Coil pacifying unit

2. The torque simulations were set up doing stationary simulations for several rotor positions. Starting with the rotor at $\Theta = -11.25$, coils within 101.25 degrees in front of the rotor (counter clockwise) where activated with rated current (10A), while every unit within 101.25 behind the rotor were

TABLE VIII: Torque at different rotor positions

Torque (Nm)				
*Rotor offset (*deg*)*	*189mm*	*179mm*	*Coils active*	*Coils passive*
-11.25	154.02	75.11	1,2,3	7,8
-5.625	147.42		1,2,3	7,8
0	137.46	58.02	2,3	7,8
5.625	140.80		2,3	1,7,8
11.25	151.59	73.26	2,3	1,7,8
16.875	156.05		2,3	1,7,8
22.5	150.93	84.66	2,3	1,8
28.125	146.11		2,3	1,8
33.75	153.77	71.91	2,3,4	1,8

pacified with rated current. This scenario is made to resemble the 'Individual control'-scheme from sec. IV. Torque was found by integrating the upward magnetic stress tensor around the rotor circumference, finding the component of the tensor tangential to the rotor in the contact point and then multiplying by machine length and rotor radius, giving the following formula.

$$T = lr_r \oint \sigma_{tang.comp} ds \tag{34}$$

$$= lr_r \oint (sin(\Theta)\sigma_y + cos(\Theta)\sigma_x) ds \tag{35}$$

$$\tag{36}$$

where σ is the magnetic stress tensor.

E. The time dependent analysis

For verification of the results found in the magnetic model-analysis, and more accurate results, a time dependent analysis would be very helpful. The model has been partly set up, but despite simplifications of the iron HB-curve, and disregarding iron losses, the study has not been solved. COMSOL-support, represented by Bertil Nistad, identified a too coarse mesh to be the problem. With a current simulation time of close to 20 hours on a regular laptop, more computing power or a lot of patience is required.

An alternative approach and possible solution is presented in an article. [6] By the creating the mesh from radial bands, the authors succeeding in solving studies with no minimum airgap. This approach should be investigated to make the time dependent study to solve.

APPENDIX D
MATLAB FILES

A set of matlab files is included as a digital appendix to this thesis on DAIM.

The matlab script used to calculate the inductances, torque and power is divided into the following parts:

Frame.m	The outer frame, decides type of calculation and resolution
ConstParam.m	Defines the constant physical parameters of the machine
Param.m	Adjusts parameters that vary with rotor position
Selfinductance.m	Defines the network to self inductance calculations
Mutualinductance.m	Defines the network to mutual inductance calculations
PMlinkage.m	Defines the network to calcuate linkage flux from PMs
Torque.m	Calculates torque from other variables

In addition, the script **nettverk.m** is called to set up the node admittance matrix from the network defined in Selfinductance.m, Mutualinductance.m and PMlinkage.m. This file is written by Svein Magne Hellesø of SINTEF, and is also included in the package.

Due to lacking understanding to lacking functionality in the nettverk.m script, or lacking understanding of the script by the author, the network has to be set up differently depending on what aspect of the flux linkage that is to be investigated. That is the reason for three different files to define the network. If one is able to get the values needed from a single node reluctance matrix, that would probably speed up the script. Generally, the script is not optimized with regards to speed.

The general language of the script is fairly basic, making it perhaps a little larger than needed to be, but hopefully possible to read.